Centro Brasileiro de Pesquisas Físicas
Coordenação de Física Teórica

Reduced-Quantum Electrodynamics in curved spaces

Pedro Igor Cavalcante Caneda

Thesis submitted in fulfillment of partial requirements for the degree of Doctor of Philosophy in Physics in the Brazilian Center for Research in Physics.

Supervisor: Gabriel Santos Menezes
Co-Supervisor: Tobias Micklitz

Rio de Janeiro - Brazil
March 2022

"REDUCED-QUANTUM ELECTRODYNAMICS IN CURVED SPACES"

PEDRO IGOR CAVALCANTE CANEDA

Tese de Doutorado em Física apresentada no Centro Brasileiro de Pesquisas Físicas do Ministério da Ciência Tecnologia e Inovação. Fazendo parte da banca examinadora os seguintes professores:

Gabriel Santos Menezes – Presidente/Orientador/CBPF

Tobias Micklitz – Coorientador/CBPF

Everton Murilo Carvalho de Abreu - UFRRJ

Humberto Belich Junior - UFES

Nami Fux Svaiter – CBPF

José Abdalla Helayel Neto - CBPF

Rio de Janeiro, 05 de maio de 2022.

Acknowledgements

Agradeço primeiramente meus orientadores Gabriel Menezes e Tobias Micklitz pelas oportunidades e apoio que me deram durante esses anos.

A minha família, especialmente a minha Mãe, Wilna Caneda, e minha tia, Wilma Caneda, por todo o apoio e suporte durante todo o caminho. Ao meu primo/irmão Thiago Caneda e meu sobrinho Benício, por todos os momentos. A Kelly por toda a força nestes anos.

Abstract

The physics of graphene has provided an important connection between quantum field theory and condensed-matter physics due to the particular features of the graphene quasiparticles which can be described as massless two-dimensional Dirac fermions. An approach that has been given promising results in this context is the reduced quantum electrodynamics. In this work we consider the natural generalization of this formalism to curved spaces. As an application, we calculate the one-loop optical conductivity of graphene taking into account the presence of curvature-inducing defects, such as disclinations and possible ripples due to thermal fluctuations. Such defects are modeled by curvature effects. When positively curved, these deffects can be incorporated locally by taking into account a suitable chemical potential, at least as far as the free fermion conductivity goes. In addition, we demonstrate how such effects may contribute to a decisive increase in the minimal conductivity.

Keywords: Quantum field theory, reduced quantum electrodynamics, graphene, curved space

Resumo

A física do grafeno forneceu uma ligação importante entre a teoria quântica de campos e a física da matéria condensada, devido às características particulares das quasipartículas do grafeno que podem ser descritas como férmions de Dirac bidimensionais não massivos. Uma abordagem que tem obtido resultados promissores nesse contexto é o da eletrodinâmica quântica reduzida. Neste trabalho consideramos a generalização natural deste formalismo para espaços curvos. Como aplicação, calculamos a condutividade ótica do grafeno a um laço, considerando a presença de curvatura induzida por defeitos, como declinações e possíveis ondulações devido a flutuações térmicas. Esses defeitos podem ser modelados por efeitos de curvatura. Quando positivamente curvados, esses defeitos podem ser incorporados localmente através de um potencial químico adequado, ao menos no caso da condutividade de férmions livres. Ainda mais, demonstramos como esses efeitos podem contribuir decisivamente para um acréscimo da condutividade mínima.

Palavras-chave: Teoria quântica de campos, eletrodinâmica quântica reduzida, grafeno, espaço curvo

Introduction

In the last decades condensed-matter systems of diverse natures have been increasingly studied under the methods of quantum field theory (QFT). This has emerged as an important tool in the condensed-matter community in the sense that QFT allows us to theoretically explore the prominent physics developing on the relevant low-energy scale probed in experiments. Remarkably, it has also been realized that elusive particles that appear in the context of high-energy physics, such as Weyl and Majorana fermions, can naturally emerge in the form of quasi-particles in a condensed-matter setting [1, 2]. On the other hand, on the footsteps of Unruh's seminal work [3] back in 1981, one has recently witnessed the outbreak of investigations dedicated to collectively understand the prospects of exploiting condensed-matter models as possible experimental realizations of physical situations that arise in the context of general relativity and of quantum field theories in curved backgrounds. For instance, it now has been well established that kinematic aspects of black holes can be investigated in weakly interacting Bose gases [4–9]. In this analog model configuration, theoretical surveys have also probed aspects of interesting kinematical effects that arise in classical and quantum systems, such as, for example, phenomena involving superradiance processes [10–17].

The investigation proposed here considers this current trend to borrow concepts originally developed in high-energy physics for the study of low-energy systems commonly found in condensed matter. We are particularly interested in the transport properties of graphene. The low-energy physics of two-dimensional carbon systems [18, 19] is governed by the presence of two generations of Dirac fermions. The electronic interactions in Dirac liquids lead to a wealth of intriguing transport phenomena [20–23] which have attracted a fair amount of attention since the first synthesization of graphene in 2004 [24]. Indeed, recent experiments uncover the relevance of such electronic interactions at low temperatures [25–28]. In turn, the interplay between strong Coulomb interactions and weak quenched disorder in graphene has also been elucidated, and the general expectation is that vector-potential disorder may play a key role in the description of transport in suspended graphene films [29]. Motivated by clear evidence of the strongly coupled nature of graphene, transport coefficients were calculated within a modern holographic setup [30].

The specific structure of the $2D$ crystal lattice permits graphene systems to be viable settings to study some of the interesting effects which arise in QFT in curved spacetimes [31–33]. In this context, measurable effects of QFT in a curved-background description of the electronic properties of graphene represent a growing ongoing line of research. A number of proposals to interpret several observed effects in graphene sheets such as curved ripples [34], corrugations [35], pure strain configurations [36] and even nonuniform elastic deformations [37] in the light of a curved-space description of the electronic properties of graphene has occupied much of the contemporary associated literature. The appearance of gauge fields in graphene systems has also made it possible to establish a firm bridge between the physics of graphene and gravity-like phenomena allowing the unification of concepts from elasticity and cosmology [38].

The chiral nature of the charge carriers in graphene is responsible for the existence of a minimal AC conductivity in the collisionless regime which is universal [39]. In this respect much theoretical effort has been devoted to understand the effects of electronic interactions on the optical conductivity in such a scenario. Despite the manifest progress toward a better comprehension of this issue, the theoretical determination of this minimal conductivity and its dependence on interactions is still a matter of intense debate (for an interesting discussion, see Ref. [40] and references cited therein). One possible framework with which one can address this issue is given by the so-called reduced quantum electrodynamics (RQED). This is a quantum field theory describing the interaction of an Abelian $U(1)$ gauge field with a fermion field living in flat spacetimes with different dimensions [41, 42]. Motivations for the investigation of such reduced theories comprise their feasible application in low-dimensional condensed-matter settings, in particular graphene systems. Indeed, it has been claimed that calculations within the formalism of RQED reproduce as close as possible the experimental results for the minimum conductivity of graphene [43]. Electromagnetic current correlation

has also been computed within the context of RQED [44]. Other interesting, noteworthy features of RQED include the validity of the Coleman-Hill theorem and the existence of quantum scale invariance [45, 46]. For recent studies of chiral symmetry breaking in RQED at finite temperature and in the presence of a Chern-Simons term, see Refs. [47, 48].

In the first chapter we introduce the physics of graphene. We focus only on those aspects that will be of interest, namely the emergence of relativistic chiral particles and the possible ways curvature can arise in graphene. We also discuss the continuum field theoretic model, Pseudo-Quantum Electrodynamics, or Reduced-Quantum Electrodynamics, appropriate for the flat graphene layer. In the second chapter we discuss the curved space generalization of the model and carry a one-loop analysis. Then we finish by applying the model to graphene, with a focus on the implications for the free fermion optical conductivity, following our work in [49].

In the present exploration our theoretical laboratory will be the generalization of the formalism of RQED to curved spaces. We do not wish to single out one particular metric in our exploration, but instead we will keep our discussion to general spatial geometries. For that we will use a momentum-space representation of the Feynman propagator in arbitrary curved spacetimes [50, 51]. As usual the construction rests upon the usage of Riemann normal coordinates [52, 53]. As an application, our discussion will allow us to calculate the one-loop high-frequency behavior of the optical conductivity in the presence of curvature effects in graphene by using the Kubo formula. We envisage these curvature effects as modelling possible ripples that may appear in graphene substrates. We will demonstrate how such effects can be incorporated by taking into account a suitable chemical potential when the Ricci scalar is positive. We will also explore the intriguing possibility that such curvature effects can actually contribute to an increase in the minimum conductivity of graphene. We employ units such that $\hbar = c = 1$.

Chapter 1

Graphene

Graphene is an one atom thick layer of graphite. It was first synthesized in laboratory in 2004 by Geim and Novoselov [24]. For their feat they were awarded the 2010 Nobel prize in physics. However it's theoretical exploration began in 1947 with Wallace as a stepping stone to understand the conduction properties of graphite [54]. A decade later the same approach was taken by McClure [55], and Slonczewski and Weiss [56] in exploring the band structure of graphite. Shortly afterwards these theoretical findings received experimental confirmation [57–61], cementing the approach originally employed by Wallace. Although graphene's characteristic conical band structure, along with it's linear dispersion, at the Brillouin zone corners had already been identified in these works it took another 16 years until the emergence of pairs of relativistic chiral Dirac excitations was first pointed out by DiVincenzo and Mele in early 1984 [62]. Later the same year Semenoff argued that the chiral nature of graphene's excitations would lead to an observable zero-energy state in an external magnetic field [63]. The zero-modes were observed by Novoselov *et al.* [18] in 2005, shortly after their pioneering manufacturing of graphene, see also [19] and [22]. This so-called anomalous quantum Hall effect amounts to a strong evidence of the relativistic chiral Dirac quasiparticles in graphene. Additionally, the observation of Klein tunneling [20, 21], in connection with backscattering suppression, adds more weight for the chiral nature of the excitations [23]. Yet another trademark feature of relativistic fermions worth mentioning is the so-called zitterbewegung [64, 65], or trembling motion, i.e., high oscilations of the wavefunction. This phenomenon has been observed for the first time for trapped ions in [66]. It is believed that graphene in a magnetic field is the best bet to observe zitterbewegung, see [67] and references therein.

The content in this section is standard and exhaustively covered throughout the literature. For greater details regarding our exposition, and many more applications, we refer to the excellent review [68]. For a more pedagogical take, see the book by Katsnelson [69].

1.1 The honeycomb lattice

Chemically graphene is a carbon allotrope with sp^2 hybridization. Three out of the four valence electrons of carbon, those from the s, p_x and p_y orbitals, are strongly bond together, the so-called σ-bonds. These are responsible for the planar honeycomb lattice structure of graphene. The fourth valence electron in the p_z orbital is only weakly bond to the others, the so-called π-bond. This is responsible for the conduction properties of graphene. Because graphene is single layer and its σ bonds are planar, it is said to be a two-dimensional material. The π-bond electron's momentum k_z perpendicular to the layer is quantized inside a very thin interval of the order $10^{-10}m$. The k_z modes are therefore widely spaced and can be taken to be frozen in it's ground state. This then completely justifies the treatment of graphene as a two-dimensional material.

The honeycomb lattice is shown in figure 1.1a. Each lattice site hosts a single conduction electron, ideal graphene is hence half-filled. Each site is connected to three others at angles of $2\pi/3$. The nearest neighbor vectors are taken as

$$\mathbf{a}_1 = \frac{a}{2}(1, \sqrt{3}), \quad \mathbf{a}_2 = \frac{a}{2}(1, -\sqrt{3}), \quad \mathbf{a}_3 = a(-1, 0), \tag{1.1}$$

where $a \approx 1.42$Å is the lattice spacing. Any two nearest sites are topologically distinct due to the different orientation to their nearest neighbors. The honeycomb lattice is therefore not a Bravais lattice, but rather is composed of two interpenetrated triangular sublattices (a bipartite lattice), commonly termed A and B,

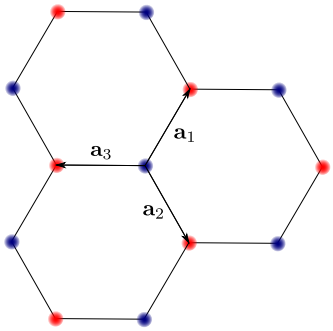

(a) Honeycomb lattice of graphene. Blue and red sites represent A and B sublattice sites. Nearest neighbors vectors $\mathbf{a}_i$ are shown.

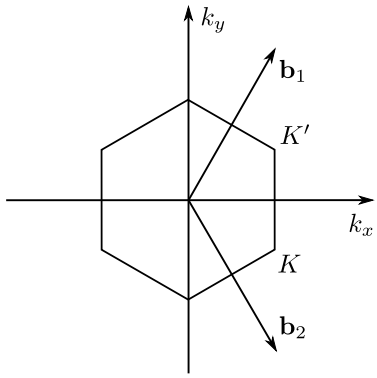

(b) 1st Brillouin zone of graphene. Reciprocal lattice vectors $\mathbf{b}_1$ and $\mathbf{b}_2$ are shown. K and K' are the special corners of the Brillouin zone where Dirac physics arises.

Figure 1.1

respectively depicted as blue and red in figure 1.1a. This sublattice structure is reponsible for the so-called pseudo-spin degree of freedom of graphene. As will be shown in the following the inherent spinorial structure of graphene's massless Dirac quasiparticles arises from it's pseudo-spin degree of freedom, rather than real spin.

To construct the first Brillouin zone of graphene the triangular lattice vectors are required, they are

$$\mathbf{r}_1 = \frac{a}{2}(3, \sqrt{3}), \quad \mathbf{r}_2 = \frac{a}{2}(3, -\sqrt{3}). \tag{1.2}$$

Then the reciprocal lattice vectors $\mathbf{b}_i$ are determined by $\mathbf{b}_i.\mathbf{a}_i = 2\pi\delta_{ij}$ yielding

$$\mathbf{b}_1 = b(1, \sqrt{3}), \quad \mathbf{b}_2 = b(1, -\sqrt{3}), \tag{1.3}$$

with $b = 2\pi/3a$. The first Brillouin Zone (BZ) can be constructed in the usual fashion and is shown in figure 1.1b. It will be shown in the following that the corners of BZ (i.e., the vertices of the hexagon) are the special points where the Dirac physics emerges. Only two out of the six corners are inequivalent, conventionally called the K and K' points, which are taken to be

$$\mathbf{K} = b\left(1, \frac{1}{\sqrt{3}}\right), \quad \mathbf{K}' = b\left(1, -\frac{1}{\sqrt{3}}\right). \tag{1.4}$$

The other corners are reached from (1.4) by linear combinations of (1.3). These points constitute yet another binary degree of freedom usually called the valley degree of freedom, or sometimes isospin. Taking into account real spin it follows that graphene excitations display a total of $2 \times 2 \times 2 = 8$ degrees of freedom. In the absence of external magnetic fields real spin plays only a spectator role, amounting just to a degeneracy factor of $g_s = 2$ on physical observables. For ideal pristine graphene there is also perfect symmetry between the valleys. In this case the total degeneracy factor is $g = g_s g_v = 4$.

1.2 Emergence of Dirac physics

The properties advertised above follow from a simple tight-binding analysis of the honeycomb lattice taking into account only nearest neighbors hopping. In this case there are couplings only between sites A and B. The Hamiltonian reads

$$H = -t \sum_{\sigma,\langle ij \rangle} (a^\dagger_{\sigma,i} b_{\sigma,j} + b^\dagger_{\sigma,j} a_{\sigma,i}), \tag{1.5}$$

where $t \approx 2.8$ eV is the overlap integral. Here $a_{\sigma,i}$, $a^\dagger_{\sigma,i}$ annihilates/creates (real) spin σ electrons at site i on sublattice A, and similarly for $b_{\sigma,j}$, $b^\dagger_{\sigma,j}$. These two independent sets of modes mean the wavefunction

has an internal degree of freedom corresponding to it's amplitude on either lattice site. This is the so-called pseudo-spin. After a Fourier transform the Hamiltonian reads, in matrix form

$$H = -t \begin{pmatrix} 0 & f(\mathbf{k}) \\ f^*(\mathbf{k}) & 0 \end{pmatrix}, \tag{1.6}$$

where

$$f(\mathbf{k}) = e^{-ik_x a} + e^{ik_x \frac{a}{2} + ik_y \frac{\sqrt{3}a}{2}} + e^{ik_x \frac{a}{2} - ik_y \frac{\sqrt{3}a}{2}}. \tag{1.7}$$

Some straightforward algebra yields the dispersion relation

$$E(\mathbf{k}) = \pm t \sqrt{3 + 2\cos(\sqrt{3}k_y a) + 4\cos\left(\frac{3k_x a}{2}\right)\cos\left(\frac{\sqrt{3}k_y a}{2}\right)} \tag{1.8}$$

The positive sign is for the conductance band and the negative for the valence band. The dispersion is shown in figure 1.2. The figure hints at the special property of (1.8), namely that the valence and conduction bands touch only at six points. These are precisely the corners of the BZ. To see that it is so it suffices to insert (1.3) for the K and K' points into (1.8) and recall that the remaining four are related to K and K' by reciprocal lattice vectors. Given the symmetry between the valence and conduction bands, it follows that the Fermi surface of half-filled graphene lies exactly at the Dirac points.

In order to uncover the linear dispersion characteristic of Dirac fermions it is only necessary to expand (1.8) around any of the corners of the BZ. This can again be anticipated by figure 1.2 noticing these points serve as a vertex to the conical shaped dispersion in their vicinity. Expanding then around the K point $\mathbf{k} = \mathbf{q} - \mathbf{K}$, $qa \ll 1$, reveals the characteristic linear dispersion of graphene

$$E(\mathbf{q}) = \pm \frac{3ta}{2}|\mathbf{q}|. \tag{1.9}$$

The coefficient is the Fermi velocity of the Dirac quasiparticles (temporarily restoring an $\hbar$ factor)

$$v_F = \frac{3ta}{2\hbar}. \tag{1.10}$$

It turns out that $v_F \approx c/300$, with c the speed of light. Graphene is therefore definitely not a strictly relativistic system. It is however relativistic-like, in the sense that (1.9) resembles the relativistic dispersion $E = \sqrt{\mathbf{q}^2c^2 + m^2c^4}$ for massless particles with the single replacement of $c \to v_F$.

The density of states per spin, per valley, near the Dirac points follows directly from counting the number of energy states using (1.9), the result is

$$\rho(\omega) = \frac{|\omega|}{2\pi v_F^2}. \tag{1.11}$$

For the full density of states, that can actually be analytically computed from (1.8), see [68]. The remarkable feature is the vanishing of the density of states precisely at the Dirac points $\omega = 0$. This is also the Fermi level in ideal graphene. For this reason graphene is frequently termed either a gapless semiconductor, or a semi-metal with vanishing density of states.

To uncover the massless Dirac quasiparticles that produce (1.9) we need to analyze the Hamiltonian (1.6) close to the Dirac points. It saves some time to absorb a global phase factor $e^{-ik_x a}$ from $f(\mathbf{k})$. It is

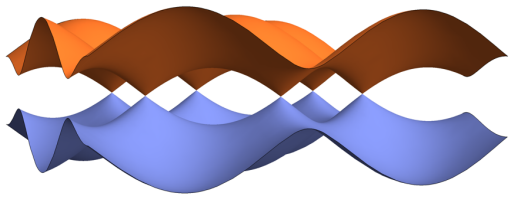

Figure 1.2: Dispersion relation of clean graphene.

also convenient to define $\mathbf{K}_\zeta = b(1, \zeta\frac{1}{\sqrt{3}})$, with $\zeta = \pm 1$, such that it corresponds to the K and K' points, respectively. Taylor expanding around the Dirac points lead to

$$f(\mathbf{q} - \mathbf{K}_\zeta) \approx -i\frac{3a}{2}(q_x - \zeta i q_y) + \mathcal{O}(q^2). \tag{1.12}$$

From (1.6) it follows the Hamiltonian H_{K_ζ} in the vicinity of the Dirac point K_ζ

$$H_{K_\zeta} = v_F \begin{pmatrix} 0 & i(q_x - \zeta i q_y) \\ -i(q_x + \zeta i q_y) & 0 \end{pmatrix}. \tag{1.13}$$

The factors of i can be removed by an unitary transformation of the base spinors. The Hamiltonian assumes the simple form

$$H_{K_\zeta} = v_F(\sigma_x q_x + \zeta \sigma_y q_y), \tag{1.14}$$

with σ_x and σ_y being the Pauli matrices. Going back to configuration space the Schrödinger equation $i\sigma_z \partial_t \psi = H_{K_\zeta}\psi$, with the Pauli matrix σ_z accounting for the positive and negative energies (1.9), becomes

$$i\sigma_z \partial_t \psi = i v_F(\sigma_x \partial_x + \zeta \sigma_y \partial_y)\psi. \tag{1.15}$$

Equation (1.15) is the massless Dirac equation. Taking $\gamma^\mu = (\sigma_z, \sigma_x, \sigma_y)$ forms a representation of the Clifford algebra $\{\gamma^\mu, \gamma^\nu\} = 2\eta^{\mu\nu}$, and allows to recast (1.15) in the familiar Dirac form

$$i v_F \gamma^\mu \partial_\mu \psi_{\zeta,\sigma} = 0, \tag{1.16}$$

where we have restored the real spin label σ for completeness, and the ζ label denotes the spinor on the respective Dirac cone. Here $\partial_\mu = (v_F^{-1}\partial_t, \boldsymbol{\nabla})$ in analogy with the usual relativistic notation, with the replacement of $c \to v_F$ for the same reasons discussed following (1.10).

The eigenfunctions $\psi_{\zeta,\sigma}$ of graphene describe chiral particles. To see this note that (1.14) is proportional to the projection of pseudo-spin along the momentum $\boldsymbol{\sigma}.\hat{\mathbf{q}}$. It follows that the energy eigenstates have definite helicity, or in this case, chirality. Therefore the spectrum of half-filled graphene around the K point consists of a right-handed positive energy particle in the conduction band and a left-handed negative energy hole in the valence band. Similarly, the spectrum around the K' point is composed of a left-handed positive energy particle (conduction band) and a right-handed negative energy hole (valence band).

It is also commonplace to consider four-dimensional spinors incorporating both Dirac points. In this case the γ-matrices can be defined by $\gamma^\mu = (\sigma_z, \sigma_x, \sigma_y) \otimes \tau_x$, where τ^i is another set of Pauli matrices acting on the valley degrees of freedom. In this case the Dirac equation is written simply

$$i v_F \gamma^\mu \partial_\mu \psi = 0, \tag{1.17}$$

where we have also dropped the real spin label σ. The physical significance of working with this representation is that it more naturally generalizes to cases where the pseudo-spin and valley symmetries are broken, e.g., by a mass term representing for instance different on-site energies between nearest neighbors.

1.3 Stability of Dirac physics

Before proceeding with a discussion of curvature inducing defects in graphene, it is sensible to understand how robust is the existence of the Dirac points over general departures from the ideal graphene monolayer. It turns out the Dirac points are pretty robust. Here we follow closely the presentation on Bernevig's book [70]. The Dirac points and cones will be lost if a perturbation causes a gap to open. A gap is tantamount to a mass term in the Dirac equation, which has the form $mv_F^2\sigma_z$. This is so because it shifts the valence band by $-mv_F^2$ and the conduction band by mv_F^2, opening a gap of energy $2mv_F^2$. Therefore the question to be answered is "When does a perturbation induce a mass term?" It will be shown in the following that the Dirac points are not only locally protected by symmetry, but also globally protected by topology. Only strong enough perturbations, in a sense to be made more precise below, may destroy the Dirac cones.

Naturally such a discussion begins with the symmetries of graphene. The honeycomb lattice has a sublattice symmetry $A \leftrightarrow B$, it does not matter how we label the sites, only that the lattice is bipartite. It has the effect of interchanging $a_{\sigma,i}^{(\dagger)} \leftrightarrow b_{\sigma,-i}^{(\dagger)}$. It is identical to an inversion about either an arbitrary lattice

site, or, more symmetrically, the center of the hexagonal rings. It imposes on a generic bipartite Hamiltonian the transformation

$$H(\mathbf{q}) = \sigma_x H(-\mathbf{q})\sigma_x \tag{1.18}$$

Including the mass term $mv_F^2\sigma_z$ in the Hamiltonian (1.14) around the Dirac points it is found

$$H_{K_\zeta}(\mathbf{q}) = v_F(-q_x\sigma_x + \zeta q_y\sigma_y - mv_F\sigma_z). \tag{1.19}$$

Recalling that $-\mathbf{K}$ is equivalent to $\mathbf{K}'$, we see that the K and K' point Hamiltonians (1.14) are mapped into each other under inversion, up to a global phase of π. More dynamically stated, hopping from pseudo-spin A to B on the K point is equivalent to hopping from pseudo-spin B to A on the K' point. Therefore a gap is consistent with inversion symmetry. More symmetry is needed.

Ideal graphene also has time-reversal symmetry, reflected on the real hopping parameter t[1]. For a generic Hamiltonian time-reversal symmetry imposes

$$H(\mathbf{q}) = H^*(-\mathbf{q}), \tag{1.20}$$

which for graphene becomes

$$H_{K_\zeta}(\mathbf{q}) = v_F(-q_x\sigma_x + \zeta q_y\sigma_y + mv_F\sigma_z). \tag{1.21}$$

It has a similar picture as for the inversion transformation. If we rewind time, then an A to B hopping becomes B to A and momentum is also inverted. However contrary to the inversion transformation (1.19), the mass term does not flip sign. For this reason it may seem that time-reversal symmetry forbids the opening of a gap. This conclusion can be avoided if the gap is momentum dependent $m = m(\mathbf{q})$. Assuming linearity around the Dirac points $m(\mathbf{q}) \sim \mathbf{q}$ would then make the mass term flip sign. Thus time-reversal too does not generally rule out the mass term.

Inversion and time-reversal symmetries alone cannot protect the Dirac points in graphene, but collectively they do. Taking both (1.18) and (1.20) together imposes on a generic Hamiltonian the condition

$$H(\mathbf{q}) = \sigma_x H^*(\mathbf{q})\sigma_x. \tag{1.22}$$

whose virtue is to constraint the Hamiltonian at any single point, as opposed to inversion (1.18) and time-reversal (1.20) transformations relating $\mathbf{q}$ to $-\mathbf{q}$. It implies that a momentum dependent mass behaves as a scalar under the combined $\mathcal{TI}$ transformation. For the same reason it does not exchange the Dirac points in graphene. Indeed, explicitly, it yields

$$H_{K_\zeta}(\mathbf{q}) = v_F(q_x\sigma_x + \zeta q_y\sigma_y - mv_F\sigma_z). \tag{1.23}$$

which does require $m = 0$. Therefore perturbations that preserve both inversion and time-reversal cannot open a gap, the Dirac physics is safe. An extension of this argument is also applicable to multilayered graphene, see [71].

An alternative topological explanation for the stability of Dirac cones in graphene makes use of the idea of Berry phases. The explicit eigenspinors for the K and K' points carry a nontrivial winding number. It follows that smooth deformations cannot destroy these vortices, unless they collide. This possibility can indeed occur under $\mathcal{TI}$ symmetric perturbations that shift the location of the Dirac points by $(\delta h_x, \zeta\delta h_y)$

$$H_{K_\zeta} + \delta H = (q_x - \delta h_x)\sigma_x + \zeta(\zeta q_y - \delta h_y)\sigma_y. \tag{1.24}$$

If h_x and h_y are tuned to join the Dirac points then the vortex-anti-vortex annihilate. In this case a gap indeed opens [70]. This however requires a large perturbation of the order of the bandwidth.

1.4 Curved graphene layers

In this short section we will quickly describe how curvature may arise in graphene layers. We will see how to account for curvature in more detail during the field theoretic discussion. Curvature has been observed to arise in both suspended graphene and upon substrates [72–80]. First of all let us point that throughout this work we will always mean intrinsic curvature, i.e., there can be no flat directions. For example, fullerene, a graphene soccer ball, is said to be curved, whereas a graphene nanotube is not.

[1] A change of basis can make t complex, however this has no physical consequence for transition probabilities.

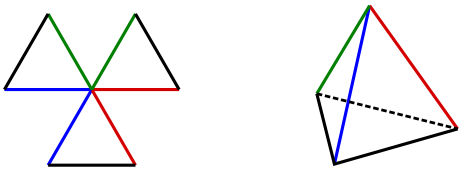

Figure 1.3

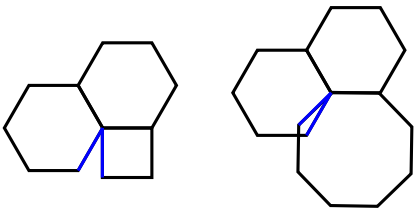

Figure 1.4: Positive and negative curvature inducing defects in graphene.

As described in [38] positive or negative curvature in graphene can arise by removing or introducing sites in a given hexagonal lattice ring. This leads to a so-called disclination. The geometrical reason disclinations lead to curvature is as follows. Three hexagons joined together as in figure 1.1a make a 2π angle at their common vertex. If we substitute a pentagon (heptagon) for a hexagon there arises a deficit (surplus) angle, leaving the lattice no option but to curve in order to stick together. This principle is illustrated in figure 1.3 for three regular triangles. If the sides with matching colors (except the black ones) are the same, the only way to compensate for the deficit angles between these sides is to curve out of the plane to make a tetrahedron. Figure 1.4 shows the analogous situation for graphene. On the left it is shown a square defect leading to a deficit angle. On the right a surplus angle arises from the octagon. For a related elegant topological argument based on the Euler characteristic of the lattice see [81]. Importantly, these lattice defects do not spoil the Dirac physics because the distortion can only be appreciated a few lattice sites away from the location of the defect. What matters for the Dirac cones to arise is the three-fold orientation between sites.

The precise relationship between defects and gravity was developed in [82]. The displacement vector field of elastic theory is approached from a geometrical standpoint as defining a diffeomorphism between ideal and deformed spaces. One is then able to define a nontrivial metric for the deformed system and bring in the tools of differential geometry and gravity. The information encoded in the Frank angle and Burges vector in the theory of elasticity is now available in the curvature $R^{\mu}{}_{\nu\alpha\beta}$ and torsion $T^{\mu}{}_{\alpha\beta}$ tensors, respectively. Disclinations are indeed found to lead to non-trivial curvature tensor but zero torsion, whereas dislocations (pairs of adjacent disclinations of opposite curvature) lead to zero curvature and non-trivial torsion tensor. A summary for quick reference is shown on table 1.1.

Finally we mention that ripples due to thermal fluctuations have also been observed [79]. In this case lattice spacings may have varying lengths. This then may also lead the lattice to curve for the same reason as before. The difference is that now the angle deficit or surplus are produced without the need of elastic defects.

Defects	**Geometry**
Elastic deformations	$R^{\mu}{}_{\nu\alpha\beta} = 0 \quad T^{\mu}{}_{\alpha\beta} = 0$
Disclinations	$R^{\mu}{}_{\nu\alpha\beta} \neq 0 \quad T^{\mu}{}_{\alpha\beta} = 0$
Dislocations	$R^{\mu}{}_{\nu\alpha\beta} = 0 \quad T^{\mu}{}_{\alpha\beta} \neq 0$
Disclinations and dislocations	$R^{\mu}{}_{\nu\alpha\beta} \neq 0 \quad T^{\mu}{}_{\alpha\beta} \neq 0$

Table 1.1: Summary of the relation between defects and geometry.

Chapter 2

Reduced-Quantum Electrodynamics in flat space

In this chapter we introduce the continuum field theory model for the electronic properties of ideal graphene. Presently the model is frequently discussed under three distinct names, which in chronological order are Pseudo-Quantum Electrodynamics, Reduced-Quantum Electrodynamics and Mixed Dimensional Quantum Electrodynamics. The general setting involves a low dimensional system hosting charged fermions, whereas the photons mediating the interactions fully permeate all dimensions. It is a widely applicable model across physics, from low dimensional systems in condensed matter to braneworld scenarios in string theory. For us the low dimensional system is graphene and the full dimensional environment is the laboratory. Independent development seems to be the reason for the multiplicity of names for the same model.

Historically it's exploration began in the late 80's by Marino [41], who baptized the model Pseudo-Quantum Electrodynamics, or PQED. In the early 90's Miransky et al. discussed the same model in [42] within the context of D-branes, wherein the name Reduced-Quantum Electrodynamics, RQED, was put forward. Mixed Dimensional Quantum Electrodynamics, or mixed QED for short, has gained space recently, specially within the conformal field theory community, probably because of the prevalence of configuration space methods in the field [83–85].

2.1 The model

From our previous discussion it is clear that the physics is described by (2+1)-dimensional chiral fermions for each valley and spin. For simplicity then we will ignore the valley and spin degrees of freedom as they play no fundamental role in the general features we wish to discuss presently. The electromagnetic interaction is mediated by the photon, which in contrast lives in (3+1) dimensions. The action of this mixed dimensional QED reads

$$S = \int d^4x \left(-\frac{1}{4} F^{\mu\nu} F_{\mu\nu} - \frac{1}{2\xi} (\partial_\mu A^\mu)^2 \right) + \int d^3x \, (i v_F \bar{\psi} \gamma^{\mu_e} \partial_{\mu_e} \psi - j^{\mu_e} A_{\mu_e}), \tag{2.1}$$

where we have adopted the standard notation, to note, $F_{\mu\nu} = \partial_\mu A_\nu - \partial_\nu A_\mu$, ξ is the gauge fixing parameter, $\bar{\psi} = \psi^\dagger \gamma^0$ is the Dirac adjoint and $j^\alpha = e\bar{\psi}_A \gamma^\alpha \psi_A = e(\bar{\psi}\gamma^0\psi, v_F \bar{\psi}\gamma^i \psi)$, with $i = 1, 2$ the fermionic current. The indices run as $\mu = 0, 1, 2, 3$ and $\mu_e = 0, 1, 2$. Sometimes this model is also referred to as $\text{QED}_{4,3}$ for the dimensions of the gauge and fermion fields, respectively. General mixed dimensional $\text{QED}_{d_\gamma, d_e}$ is also frequently considered in the literature, both from a purely formal perspective to access generic features of the model, as well as to applications for other dimensionally reduced systems, like nanowires or boundaries of topological insulators [86]. Due to our focus on graphene in this work, mixed QED will always implicitly mean $\text{QED}_{4,3}$.

Action (2.1) has two unique properties compared to standard QED. First the momentum in the orthogonal direction to the graphene plane, p_3 for definiteness, plays no role. As discussed previously for the electrons in graphene, it is quantized with huge level spacing, rendering it frozen in it's lowest value at all times for typical probed energies in condensed matter settings. In this case the interaction vertex cannot scatter p_3. This implies then that loops of virtual intermediate states do not include any p_3 integral. p_3 is effectively an inert degree of freedom. Secondly, note that the gauge field A_3 does not participate in the interaction

vertex. It is merely a spectator free field tagging along. Graphene physics therefore can be described solely by three-dimensional fields and momenta. This is indeed reflected in both the Feynman rules for the theory and the resulting effective field theory model. The reduction process going from the mixed dimensional model to the purely three-dimensional model by properly removing these sterile degrees of freedom was detailed in [41], which we follow.

The reduction affects only the gauge field terms as it is where p_3 or A_3 appear. It is useful however to rewrite everything in $(3+1)d$ First express the current as

$$j^{\mu}(x^0,x^1,x^2,x^3)=\begin{cases} j^{\mu_e}(x^0,x^1,x^2)\delta(x^3), & \mu=\mu_e=0,1,2 \\ 0, & \mu=3. \end{cases} \tag{2.2}$$

This allows to write all terms with the gauge field under the (3+1)-dimensional integral. The partition function of the theory is

$$Z=\int \mathcal{D}\psi\mathcal{D}\bar{\psi}\mathcal{D}A_{\mu}e^{iS[\psi,\bar{\psi},A]+iS[\psi,\bar{\psi}]}, \tag{2.3}$$

with

$$S[\psi,\bar{\psi},A]=\int d^3xdx^3\left(\frac{1}{2}A_{\mu}\left(\Box\eta^{\mu\nu}+\partial^{\mu}\partial^{\nu}\right)A_{\nu}+j^{\mu}A_{\mu}\right), \tag{2.4}$$

and $S[\psi,\bar{\psi}]$ the three-dimensional free fermion action. $S[\psi,\bar{\psi},A]$ is quadratic and so A_{μ} can be readily integrated out in the partition function

$$Z=\int \mathcal{D}\psi\mathcal{D}\bar{\psi}\exp\left(\frac{1}{2}\int d^3xdx^3d^3x'dx'^3\,j^{\mu}(x,x^3)D_{\mu\nu}(x-x',x^3-x'^3)j^{\nu}(x',x'^3)\right)e^{iS[\psi,\bar{\psi}]}, \tag{2.5}$$

where $D_{\mu\nu}(x-x',x^3-x'^3)$ is the gauge field propagator

$$D_{\mu\nu}(x-x',x^3-x'^3)=\int\frac{d^3q}{(2\pi)^3}\frac{dq_3}{2\pi}\frac{1}{q^2+q_3^2}\left(\eta_{\mu\nu}-\left(1-\frac{1}{\xi}\right)\frac{q_{\mu}q_{\nu}}{q^2+q_3^2}\right)e^{iq.(x-x')+iq_3(x^3-x'^3)}. \tag{2.6}$$

Making use of the Dirac deltas $\delta(x^3)$, $\delta(x'^3)$ in the currents kill the x^3 and x'^3 integrals and wipe out all dependence on them. What's left is the momentum q_3 on the gauge propagator (2.6). Momentum-space current conservation $q_{\mu}j^{\mu}=0$ allows us to drop the longitudinal term on (2.6), leaving only the gauge-independent contribution

$$D_{\mu_e\nu_e}(x-x')=\eta_{\mu_e,\nu_e}\int\frac{d^3q}{(2\pi)^3}\frac{dq_3}{2\pi}\frac{e^{iq.(x-x')}}{q^2+q_3^2}, \tag{2.7}$$

which can also be integrated exactly, yielding

$$D_{\mu_e\nu_e}(x-x')=\eta_{\mu_e\nu_e}\frac{i}{2}\int\frac{d^3q}{(2\pi)^3}\frac{e^{iq.(x-x')}}{\sqrt{q^2}}. \tag{2.8}$$

The gauge propagator (2.8) contains only three-dimensional quantities.

Together with the remaining, unaltered, momentum-space Feynman rules for the fermion and interaction vertex in QED we have

$$D_{\mu\nu}(q)=\frac{1}{2\sqrt{q^2}}\left(\eta_{\mu\nu}-(1-\tilde{\xi})\frac{q_{\mu}q_{\nu}}{q^2}\right) \tag{2.9a}$$

$$iS(k)=i\frac{\gamma^0\omega+v_F\boldsymbol{\gamma}.\mathbf{k}}{\omega^2-v_F^2k^2} \tag{2.9b}$$

$$-ie\Gamma_0^{\mu}=-ie\gamma^{\mu}=-ie(\gamma^0,v_F\boldsymbol{\gamma}). \tag{2.9c}$$

These are the Feynman rules of mixed QED. The reduction process is now formally complete. The set of Feynman rules (2.9) is commonly known as Reduced Quantum Electrodynamics (RQED) [42, 44]. Notice the gauge fixing parameter $\tilde{\xi}$ appearing in (2.9) is in general different from the ξ in (2.1). Gauge choices are always meant with respect to $\tilde{\xi}$, e.g., the Feynman gauge adopted throughout means $\tilde{\xi}=1$, which in turn will not correspond to the $\xi=1$ Feynman gauge in (2.1).

We notice that it is possible to reverse engineer (2.9) and explicitly write down a purely (2+1)-dimensional action

$$S_{\text{PQED}} = \int d^3x \left(-\frac{1}{2} F_{\mu\nu} \frac{1}{\sqrt{-\Box}} F^{\mu\nu} - \frac{1}{2\tilde{\xi}} \frac{(\partial_\mu A^\mu)^2}{\sqrt{-\Box}} + i\bar{\psi} \not{D} \psi \right). \tag{2.10}$$

In this form the theory is known as Pseudo-Quantum Electrodynamics, or PQED, on account of the pseudo-differential operator $(-\Box)^{-1/2}$. Do take note that we commit a harmless abuse of notation here. The gauge field A_μ in (2.10) is not the same as in (2.1). The latter was integrated out, while the former was defined so as to reproduce it's physical features in a reduced number of dimensions. The context easily distinguishes them so no confusion should arise. Furthermore the covariant derivative is defined $D_\mu = \partial_\mu - ieA_\mu$ and the Feynman slash notation $\not{D} = \gamma^\mu \partial_\mu$ is employed.

Action (2.10) is non-local. Non-local models usually suffer from many issues. Non-locality itself poses interpretation issues seemingly in conflict with basic principles of quantum field theory. At first however such issues does not appear to be too serious as PQED is not a fundamental theory. Nevertheless there has been many efforts to establish PQED as a sensible theory. The pseudo-differential operator itself was carefully discussed in [87]. Canonical quantization and asymptotic states of nonlocal theories were discussed in [88, 89]. In [90] it was found that PQED is indeed an unitary theory. Standing on a solid basis, PQED is being increasingly explored, extended and applied. Some examples, by no means exhaustive, include bosonic interactions [91], chiral symmetry breaking [92, 93], Proca electrodynamics [94], dynamical mass generation [95], cavity effects [96], Pseudo-Chern-Simons extension [97, 98] and many more.

So far we have presented mixed QED, RQED and PQED. They are all physically equivalent up to the erasure of the trivial x^3 dependence and the free A_3 field. The only element that could distinguish between mixed QED and RQED/PQED would be the excitation of higher p_3 modes of the electrons in graphene, but that is ruled out for realistic experiments. More theoretically this would be completely justified for a brane model. In this case the fermions are restricted to a zero thickness brane, whereas the gauge fields permeate the entire space. This is indeed the context whence RQED was discussed in [42].

Although equivalent it will prove useful to make a formal distinction between them. For now this will be purely a matter of nomenclature. Throughout this work we will call the set of Feynman rules (2.9) alone RQED. On the other hand, action (2.10) will be called PQED. The motivation for this distinction is that for curved spaces it seems possible to generalize (2.9), under some hypothesis to be discussed opportunely, whereas (2.10) seems to resist any attempts to such generalizations so far. Finally mixed (dimensional) QED will stand exclusively for (2.1). When discussing general features we will collectively refer to any one of these theories simply as the model.

2.2 Features of the model

The model enjoys some striking features in contrast with usual four-dimensional QED. A discussion of these features is therefore desirable to better familiarize with the model.

First of all we observe, importantly, that the reduced photon propagator (2.9a) reproduces the familiar $1/r^2$ Coulomb interaction in the $(2+1)d$ graphene layer. It can be readily anticipated on grounds of dimensional analysis: from the gauge propagator $\propto \int d^3q \sqrt{q^{-2}}$ has dimensions of $[E]^{-2}$. This is in stark contrast with the $1/r$ interaction predicted by QED_3. The standard $1/r^2$ is clearly the correct power-law for planar condensed matter systems as it lives itself in the three-dimensional laboratory.

Still within the theme of dimensional analysis we carry out a power counting analysis on (2.1). The kinetic terms for the gauge and fermion fields give $[A_\mu] = [\psi] = 1$. This already differs from QED, where $[\psi] = 3/2$, due to the low dimensionality of the fermions. This in turn implies that the coupling constant is dimensionless $[e] = 0$ as it only shows up in the low dimensional sector. The electromagnetic interaction therefore remains marginal at tree-level in mixed QED. Naturally this can also be done on PQED (2.10) with the same outcome: the lower dimensionality in the gauge kinetic term is compensated by the square-root of the d'Alembertian sitting at the denominator.

The vanishing of scaling dimension of the coupling $[e] = 0$ causes the beta function in mixed QED to vanish at the classical level. So far this is the same as in QED_4. It turns out however that contrary to QED_4, quantum corrections in mixed QED are UV finite and therefore

$$\beta_e = 0. \tag{2.11}$$

(2.11) has been verified at the two-loop level by Teber [44] . This hints towards an emerging scale invariance in mixed QED, which has subsequently been proved in [99]. A frequent argument made for the conformal invariance of mixed QED points that the renormalization of the coupling e happens only on the three-dimensional plane. Furthermore the Ward identity ties the photon's wavefunction renormalization to that of the electric charge e. However due to the local nature of UV divergences it cannot be that e is renormalized away from the plane. In this case the photon's wavefunction would renormalize on the plane, but not anywhere else. This inconsistency can only be avoided if e does not renormalize at all, hence $\beta_e = 0$ exactly. This result will be verified to one-loop level in the next section.

So far we have left the Fermi velocity v_F out of the discussion, i.e., the considerations so far apply only to the relativistic limit $v_F = 1$ of mixed QED. In the non-relativistic domain of graphene (in the strict sense of $v_F < 1$) the story gets new twists. First and foremost, $[v_F] = [E]^0$ for being a velocity. Alternatively from (1.10) we see that it v_F is the product of an energy t with a length a, hence dimensionless in natural units. However

$$\beta_v > 0, \tag{2.12}$$

that is, interactions renormalize the Fermi velocity up. The renormalization of v_F has been extensively discussed in the literature [100]. Most important is that the running of v_F ends on a fixed point at the speed of light $v_F = c$ as it should. More details on the renormalization in graphene can be found in [101, 102].

The running of v_F enables the fine-structure constant of graphene

$$\alpha_v = \frac{e^2}{4\pi v_F} \tag{2.13}$$

to run despite the fact that $\beta_e = 0$ The flow here is in the opposite direction of QED_4, as v_F increases in the UV, α_v decreases. An important observation is that for graphene $\alpha_v \approx 2.2$. Therefore mixed QED applied to graphene looks like a strongly coupled theory. Nonetheless it has been shown by Das Sarma et al. in [103] that the multiplicity of fermionic states in graphene effectively suppresses non-leading order corrections, effectively rendering perturbation theory applicable.

2.3 Renormalization

To formalize much of the discussion, let us introduce the renormalized parameters

$$\begin{aligned} \psi &= Z_2^{1/2}\psi_R \\ A_\mu &= Z_3^{1/2}A_{R,\mu} \\ e &= Z_e e_R \\ v &= Z_v v_R \end{aligned} \tag{2.14}$$

The subscript R denotes the renormalized quantities. To avoid clutter we suppress the F subscript of the Fermi velocity, i.e., $v_F \to v$. The PQED action in the Feynman gauge $\tilde{\xi} = 1$ (2.10) then becomes

$$S = \int d^3x \left[-\frac{Z_3}{2}\frac{F_{R,\mu\nu}F_R^{\mu\nu}}{\sqrt{-\Box}} + iZ_2\bar{\psi}_R\left(\gamma^0(\partial_0 - iZ_e\sqrt{Z_3}e_R A_{R,0}) + Z_v v_R\gamma^i(\partial_i - iZ_e\sqrt{Z_3}e_R A_{R,i})\right)\psi_R \right], \tag{2.15}$$

with the renormalized field strength $F_R^{\mu\nu} = \partial^\mu A_R^\nu - \partial^\nu A_R^\mu$. The computation of the Z's goes almost identically as in QED, with the exception that now frequency and momentum parts renormalize differently because the latter picks an extra factor of Z_v. Therefore it proves useful to parametrize the fermion self-energy and the vertex corrections as follows

$$-i\Sigma(\omega_k, \mathbf{k}) = -i\Sigma_\omega(\omega_k, \mathbf{k})\gamma^0\omega - i\Sigma_k(\omega_k, \mathbf{k})v\boldsymbol{\gamma}.\mathbf{k} \tag{2.16a}$$

$$-ie\Gamma^\mu(0,0) = -ie\left(\Gamma_\omega\gamma^0, \Gamma_k v\gamma^i\right). \tag{2.16b}$$

Here we skip the vacuum polarization for expediency, as we know already it does not renormalize (a fact we will verify shortly). The renormalization parameters δZ_n, with $n = 1, 2, 3, e, v$ a general label, defined

$$Z_n = 1 + \delta Z_n + \mathcal{O}(\alpha_v^2), \tag{2.17}$$

are responsible for cancelling the UV divergences in the one-loop functions. Whereas the frequency parts go just like QED, e.g., $\Sigma_{1\omega}$ (the 1 indicates the one-loop approximation) has its UV divergence cancelled by δZ_2, the spatial part Σ_{1k} contains an extra δZ_v which may be obtained as the residual UV divergence after the subtraction of the one from $\Sigma_{1\omega}$. Put into equations this simply means

$$\delta Z_2 = \Sigma^{\rm UV}_{1\omega} \tag{2.18a}$$

$$\delta Z_v = \Sigma^{\rm UV}_{1k} - \Sigma^{\rm UV}_{1\omega}\,. \tag{2.18b}$$

where the UV label denotes we're considering only the UV divergent part of the function. In the same fashion we find the same result for the vertex corrections as well

$$\delta Z_2 = \Gamma^{\rm UV}_{1\omega} \tag{2.19a}$$

$$\delta Z_v = \Gamma^{\rm UV}_{1k} - \Gamma^{\rm UV}_{1\omega}\,. \tag{2.19b}$$

Agreement between (2.18) and (2.19) serves as a consistency check for the model both in flat and curved spaces, hence we will dedicate some time to verifying their equality.

We observe that the Ward Identity

$$Z_1 = Z_2 \tag{2.20}$$

still holds, as argued above. To verify this one must consistently compare the frequency (momentum) part of the vertex renormalization Z_1 with it's respective frequency (momentum) counterpart in the electron wavefunction renormalization Z_2. Thus the well-known connection between the photon's wavefunction and electric charge renormalizations follow

$$Z_e = Z_3^{-1/2}. \tag{2.21}$$

The issue of gauge invariance and the Ward Identity may be a bit more involved in curved spaces, specially so for RQED. We will come back to it in due time in the next chapter.

2.4 Predictions of the model

In this section we discuss some of the predictions of the model. The results presented here have all been obtained already in the literature. It's value here is to set the stage for future reference for the curved space generalization.

2.4.1 Density of States

One particular observable that can be readily computed, and will be of interest later when we introduce curvature, is the free fermion density of states. It is given by the retarded fermion propagator as [105]

$$\rho(\omega) = -\frac{1}{\pi}\mathrm{Im}\int d^2\mathbf{k}\,\mathrm{Tr}\left[S_0(\omega+i\epsilon,\mathbf{k})\gamma^0\right], \tag{2.22}$$

where Tr is the trace over the Dirac matrices. By virtue of $\mathrm{Tr}[\gamma^\mu\gamma^\nu] = 2\eta^{\mu\nu}$, the trace vanishes when $\mu \neq \nu$, leaving only the frequency term of (2.9b) to contribute

$$\rho(\omega) = -\frac{\omega}{\pi}\mathrm{Im}\int d^2\mathbf{k}\,\frac{1}{\omega^2 - v^2\mathbf{k}^2}. \tag{2.23}$$

The imaginary part of this integral can be computed by the standard identity

$$P\left(\frac{1}{x\pm i\epsilon}\right) = \frac{1}{x} \mp i\pi\delta(x), \tag{2.24}$$

furnishing

$$\rho(\omega) = \frac{\omega}{\pi}\int_0^\infty dk\,k\,\delta(\omega^2 - v^2\mathbf{k}^2) = \frac{\omega}{2\pi v^2}, \tag{2.25}$$

by use of standard delta function identities. To account for spin and valley degeneracy in graphene one must multiply (2.25) by the degeneracy factor $g_s g_v = 4$. It agrees with (1.11) as it should.

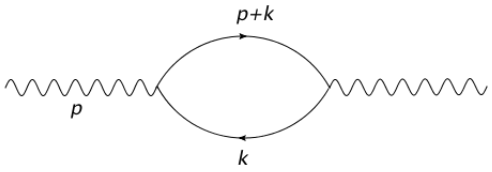

Figure 2.1: Photon's 1 loop vacuum polarization.

2.4.2 Optical Conductivity

The conductivity tensor $\sigma^{\mu\nu}$ can be computed in linear response theory as the response to external electromagnetic field. A famous formula by Kubo links the conductivity to the photon's vacuum polarization tensor $\Pi^{\mu\nu}$ as

$$\sigma^{\mu\nu}(\omega) = \lim_{\mathbf{p}\to 0} \frac{i\Pi^{\mu\nu}(\omega, \mathbf{p})}{\omega + i\epsilon}. \tag{2.26}$$

For a derivation of (2.26) see [104].

The goal then is to compute the vacuum polarization, shown in figure 2.1. To one-loop level it is

$$i\Pi^{\mu\nu}(p) = -\int \frac{d^3k}{(2\pi)^3} \mathrm{Tr}\left[iS_0(k)(-ie\Gamma_0^\mu)iS_0(p+k)(-ie\Gamma_0^\nu)\right]. \tag{2.27}$$

The computation is entirely analogous to that of QED. Notice that there are no internal photon lines in the bubble of figure 2.1 and correspondingly no photon propagator in (2.27). It follows that the result is identical to that in QED_3. The distinction between mixed QED and QED_3 can be accessed only at the two-loop level and higher (when it comes to the vacuum polarization). More physically this can be quickly understood from the fact that the one-loop contribution accounts for the free-fermion conductivity. Electron-electron interaction effects start at two-loops through the appearance of internal photon lines.

This consideration indicates that the minimum conductivity is independent of the Fermi velocity v_F. To see this first write (2.27) explicitly

$$i\Pi^{\mu\nu}(p) = -e^2 \int \frac{d\omega_k}{2\pi} \frac{d^2\mathbf{k}}{(2\pi)^2} \frac{\mathrm{Tr}[\gamma^\alpha\gamma^\mu\gamma^\beta\gamma^\nu]k_\alpha(p+k)_\beta}{(\omega_k^2 - v^2\mathbf{k}^2)((\omega_k+\omega_p)^2 - v^2(\mathbf{k}+\mathbf{p})^2)}. \tag{2.28}$$

Rescaling the spatial momenta $\mathbf{k} \to v_F\mathbf{k}$ should factor an overall v_F^{-2} factor off the integral. However the longitudinal conductivity is encoded in the $\mu = \nu = i$, which itself contributes exactly a factor of v_F^2 coming from the spatial component of the interaction vertices. A residual v_F dependence survives together with the external momentum $v_F\mathbf{p}$, but this then vanishes in the local limit in (2.26). This exact cancellation disappears from two-loops and higher, once the internal photon lines with the speed of light $c = 1$ enter the diagram, providing a new dimensionless parameter v_F/c. We will see this arises in the remaining one-loop diagrams for the self-energy and vertex correction.

For the limit of interest in (2.26), we can deal with the relativistic analog of (2.27) without losing anything

$$i\Pi^{\mu\nu}(p) = -2e^2 \int \frac{d^3k}{(2\pi)^3} \frac{k^\mu(p+k)^\nu + k^\nu(p+k)^\mu - k.(p+k)\eta^{\mu\nu}}{k^2(p+k)^2}, \tag{2.29}$$

where we have made use of $\mathrm{Tr}[\gamma^\alpha\gamma^\mu\gamma^\beta\gamma^\nu] = 2(\eta^{\alpha\mu}\eta^{\beta\nu} - \eta^{\alpha\beta}\eta^{\mu\nu} + \eta^{\alpha\nu}\eta^{\beta\mu})$. This loop integral is standard and can be quickly solved by introducing Feynman parameters and symmetry considerations. One finds

$$i\Pi^{\mu\nu}(p) = -2e^2 \int_0^1 dx \int \frac{d^3k}{(2\pi)^3} \frac{1}{(k^2-\Delta)^2} \left(-\frac{1}{3}k^2\eta^{\mu\nu} + x(1-x)(p^2\eta^{\mu\nu} - 2p^\mu p^\nu)\right), \tag{2.30}$$

where $\Delta = \sqrt{-x(1-x)p^2}$. There are two different loop integrals which in DR evaluate to

$$\int \frac{d^dk}{(2\pi)^d} \frac{k^2}{(k^2-\Delta)^2} = \frac{i(-1)^{-1}}{(4\pi)^{d/2}} \frac{1}{\Delta^{1-d/2}} \frac{\Gamma\left(1+\frac{d}{2}\right)\Gamma\left(1-\frac{d}{2}\right)}{\Gamma(2)\Gamma\left(\frac{d}{2}\right)} \tag{2.31}$$

$$\int \frac{d^dk}{(2\pi)^d} \frac{1}{(k^2-\Delta)^2} = \frac{i(-1)^{-2}}{(4\pi)^{d/2}} \frac{1}{\Delta^{2-d/2}} \frac{\Gamma\left(\frac{d}{2}\right)\Gamma\left(2-\frac{d}{2}\right)}{\Gamma(2)\Gamma\left(\frac{d}{2}\right)}. \tag{2.32}$$

Notice that for $d \to 3-2\epsilon$ neither are UV divergent. This confirms what has been previously stated about the UV finiteness of Z_3 and Z_e as promised. After a bit of elementary algebra we find

$$i\Pi_1^{\mu\nu}(p) = -\frac{e^2}{2\pi}\frac{p^2\eta^{\mu\nu} - p^\mu p^\nu}{\sqrt{p^2}}\int_0^1 dx\sqrt{x(1-x)}. \tag{2.33}$$

It has the expected structure for the vacuum polarization, it is explicitly transverse and comes with the characteristic $1/\sqrt{p^2}$ factor of PQED.

Finally for the limit (2.26) it is found for the longitudinal conductivity

$$\lim_{\mathbf{p}\to 0}\frac{i\Pi^{ij}}{\omega} = \frac{e^2}{\pi}\int_0^1 \sqrt{x(1-x)}\eta^{ij}. \tag{2.34}$$

The integral evaluates to $\pi/8$, leading to a finite longitudinal conductivity per spin, per valley

$$\sigma = \frac{e^2}{4}. \tag{2.35}$$

It is worth pointing out that there has been some confusion in the literature regarding the minimal conductivity of graphene. This is neatly summarized in Teber's thesis [40].

For the two-loop computation, see Teber [44]. A discussion about the conductivity up to two-loops can be found in Marino [43]. Ordinarily electron-electron interactions have no impact in the conductivity, this is usually a role played by disorder. The reason being that typically momentum conservation directly implies velocity, and thus current, conservation. This is the content of the so-called Kohn's theorem [106]. However for graphene, and Dirac materials in general, there is no such connection, all electrons travel at the Fermi velocity regardless of their momentum. As pointed out in [107] this allows for electron-electron interactions, i.e., higher-loop contributions to the vacuum polarization, to affect the conductivity.

Notice that the off-diagonal elements vanish because (2.34) is proportional to the metric tensor. Hall conductivity can be obtained from the inclusion of a Chern-Simons term to the action of PQED. In [108] it is shown that this is in turn one-loop exact, i.e., no higher-order corrections arise. This is a consequence of the topological nature of Hall physics and so is expected to remain unaltered in curved spaces discussed later on this work as long as the topology is not modified.

2.4.3 Running of the Fermi velocity

The Fermi velocity renormalization can be seen from the fermionic self-energy or the vertex correction. Indeed the Ward Identity guarantees that these should match. It turns out to be simpler to compute the fermionic self-energy, to which we now turn. In the next subsection we will confirm that the Ward Identity holds in mixed QED by computing the UV-diverging part of the vertex correction. Contrary to the vacuum polarization, both these diagrams involve internal photon lines and so are not related to the corresponding QED_3 diagrams. This then constitutes a legitimate non-trivial test of the inner consistency of mixed QED and for this reason we will be more detailed in the computation.

The fermion self-energy is shown in figure 2.2 and translates to

$$-i\Sigma_1(k) = \int\frac{d^3q}{(2\pi)^3}(-ie\Gamma_0^\mu)iS_0(k-q)(-ie\Gamma_0^\nu)iD_{0,\mu\nu}(q). \tag{2.36}$$

The computation uses the standard manipulations. To deal with the UV divergencies we will use dimensional regularization (DR), which shall be employed throughout this work. Our convention for DR is to take $d = 3-2\epsilon$, which then makes the charge scale as $\mu^{\epsilon/2}e$. The loop-integrals are somewhat more involved than in the bubble diagram due to the presence of the photon propagator as mentioned previously, explicitly

$$-i\Sigma_1(k) = -\frac{\mu^\epsilon e^2}{2}\int\frac{d^{d-1}\mathbf{q}}{(2\pi)^{d-1}}\frac{d\omega_q}{2\pi}\frac{\gamma^\mu(\gamma^0(\omega_k-\omega_q) - v\boldsymbol{\gamma}.(\mathbf{k}-\mathbf{q}))\gamma_\mu}{((\omega_k-\omega_q)^2 - v^2(\mathbf{k}-\mathbf{q})^2)(\omega_q^2+\mathbf{q}^2)^{1/2}}. \tag{2.37}$$

The safest way to navigate these loops is to first do the frequency integration. Notice that in this case it is a $d=1$ integral and is UV finite. The result is

$$-i\Sigma_1(k) = -\frac{\mu^\epsilon e^2}{4\pi}\int_0^1 dx\frac{1}{\sqrt{1-x}}\int\frac{d^{d-1}\mathbf{q}}{(2\pi)^{d-1}}\frac{\gamma^0(1-x)\omega_k + v\boldsymbol{\gamma}.(\mathbf{k}-\mathbf{q})}{x(1-x)\omega_k^2 + xv^2(\mathbf{k}-\mathbf{q})^2 + (1-x)\mathbf{q}^2}, \tag{2.38}$$

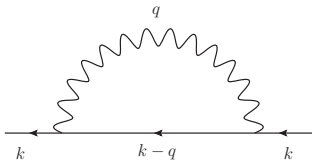

Figure 2.2: Fermion's 1 loop self-energy.

with x being a Feynman parameter. The integral can be manipulated into the more pleasant form

$$-i\Sigma_1(k) = -\frac{\mu^\epsilon e^2}{4\pi}\int_0^1 dx \frac{\sqrt{1-x}}{1-x(1-v^2)}\int \frac{d^{d-1}\mathbf{q}}{(2\pi)^{d-1}}\frac{\gamma^0\omega_k + \frac{v}{1-x(1-v^2)}\boldsymbol{\gamma}.\mathbf{k}}{\mathbf{q}^2-\Delta}, \tag{2.39}$$

where

$$\Delta = x(1-x)\left(\frac{\omega_k^2}{1-x(1-v^2)} + \frac{v^2\mathbf{k}^2}{(1-x(1-v^2))^2}\right). \tag{2.40}$$

From equation (2.39) we can write down useful expressions for the parameters $\Sigma_{1\omega}$ and Σ_{1k} appearing in (2.16) for the frequency and momentum parts of the self-energy

$$-i\Sigma_{1\omega} = -\frac{\mu^\epsilon e^2}{4\pi}\int_0^1 dx \frac{\sqrt{1-x}}{1-x(1-v^2)}\int \frac{d^{d-1}\mathbf{q}}{(2\pi)^{d-1}}\frac{1}{\mathbf{q}^2-\Delta} \tag{2.41a}$$

$$-i\Sigma_{1k} = -\frac{\mu^\epsilon e^2}{4\pi}\int_0^1 dx \frac{\sqrt{1-x}}{(1-x(1-v^2))^2}\int \frac{d^{d-1}\mathbf{q}}{(2\pi)^{d-1}}\frac{1}{\mathbf{q}^2-\Delta}. \tag{2.41b}$$

The loop integral is the same in both cases

$$\int \frac{d^{d-1}\mathbf{q}}{(2\pi)^{d-1}}\frac{1}{\mathbf{q}^2-\Delta} = \frac{i(-1)^{-1}}{(4\pi)^{\frac{d-1}{2}}}\frac{1}{\Delta^{1-\frac{d-1}{2}}}\frac{\Gamma\left(\frac{d-1}{2}\right)\Gamma\left(1-\frac{d-1}{2}\right)}{\Gamma(1)\Gamma\left(\frac{d-1}{2}\right)} \tag{2.42}$$

and it is indeed UV divergent this time when $d \to 3-2\epsilon$. The UV divergences are therefore given by

$$\Sigma_{1\omega}^{\text{UV}} = -\frac{e^2}{16\pi^2}\int_0^1 dx \frac{\sqrt{1-x}}{1-x(1-v^2)} \tag{2.43a}$$

$$\Sigma_{1k}^{\text{UV}} = -\frac{e^2}{16\pi^2}\int_0^1 dx \frac{\sqrt{1-x}}{(1-x(1-v^2))^2}. \tag{2.43b}$$

Under the condition that $v^2 \leq 1$, within the physically allowed interval, the integrals can be done and the results are finally given by

$$\Sigma_{1\omega}^{\text{UV}} = \frac{e^2}{16\pi^2}\frac{2}{1-v^2}\left(1-\frac{v\cos^{-1}v}{\sqrt{1-v^2}}\right) \tag{2.44a}$$

$$\Sigma_{1k}^{\text{UV}} = -\frac{e^2}{16\pi^2}\frac{1}{1-v^2}\left(\frac{\cos^{-1}v}{v\sqrt{1-v^2}}-1\right). \tag{2.44b}$$

Equation (2.44a) gives the renormalization of the fermion wavefunction

$$\delta Z_2 = \frac{e^2}{8\pi^2}\left(\frac{1}{1-v^2}-\frac{v\cos^{-1}v}{(1-v^2)^{3/2}}\right). \tag{2.45}$$

whose discussion will be postponed. Subtracting (2.44a) from (2.44b) one obtains δZ_v according to (2.18b)

$$\delta Z_v = -\frac{\alpha_v}{4\pi}\left(\frac{3v}{1-v^2}-\frac{(1+2v^2)\cos^{-1}(v)}{(1-v^2)^{3/2}}\right). \tag{2.46}$$

The beta function β_v that follows from (2.46) is shown in figure 2.3. It is clear that the β_v approaches a fixed point as $v \to 1$.

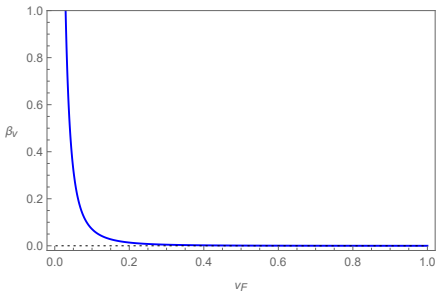

Figure 2.3: Fermi velocity 1-loop beta function.

2.4.4 β_v from vertex

We can obtain the same result from the UV behavior of the one-loop correction to the vertex function. We emphasize that this serves primarily as a consistency check for the model. Figure 2.4 shows the diagram for the one-loop vertex correction. We will compute the time and spatial components separately, beginning with the former which is given by

$$-ie\Gamma_1^0(k_1,k_2) = \int \frac{d^3q}{(2\pi)^3}(-ie\Gamma_0^0)iS_0(k_1+k)(-ie\Gamma_0^0)iS_0(k_2+k)(-ie\Gamma_0^0)iD_{0,00}(k). \tag{2.47}$$

For the UV behavior we evaluate (2.47) at zero externa momenta, $k_1 = k_2 = 0$. The one-loop vertex correction then takes the form

$$-ie\Gamma_1^0 = \gamma^0\frac{e^3}{2}\int\frac{d^{d-1}\mathbf{k}}{(2\pi)^{d-1}}\int\frac{d\omega_k}{2\pi}\frac{\omega_k^2+v^2\mathbf{k}^2}{(\omega_k^2-v^2\mathbf{k}^2)^2(\omega_k^2-\mathbf{k}^2)^{1/2}}. \tag{2.48}$$

Notice that a potential term proportional to $\boldsymbol{\gamma}$ drops out because of symmetry considerations, it comes out as a mixed $\omega_k\mathbf{k}$ contribution in the loop momenta.

The loop integrals are done in the same fashion as that detailed for the one-loop self-energy diagram. Introducing a Feynman parameter and doing the frequency integral first is straightforward

$$-ie\Gamma_1^0 = -\gamma^0\frac{e^3}{8\pi}\int_0^1 dx\frac{x}{\sqrt{1-x}}\frac{(1-x)(1-v^2)-v^2}{(1-x(1-v^2))^2}\int\frac{d^{d-1}\mathbf{k}}{(2\pi)^{d-1}}\frac{1}{\mathbf{k}^2}. \tag{2.49}$$

Notice that again there is no UV divergence from the frequency integral, so the it must come from the momentum integration. Additionally there is also an infrared divergence that can be regulated in the usual way. Focusing only on the UV divergence we find for $\Gamma_{1\omega}$ defined in (2.16)

$$\Gamma_{1\omega} = \frac{-e^2}{32\pi^2}\int_0^1 dx\frac{x}{\sqrt{1-x}}\frac{(1-x)(1-v^2)-v^2}{(1-x(1-v^2))^2}. \tag{2.50}$$

Finally

$$\delta Z_2 = \frac{e^2}{8\pi^2}\left(\frac{1}{1-v^2}-\frac{v\cos^{-1}(v)}{(1-v^2)^{3/2}}\right). \tag{2.51}$$

This agrees exactly with (2.44a) for the fermion wavefunction renormalization as anticipated on physical grounds. This consists in the first positive consistency check of the Ward Identity in mixed QED.

To compute now the renormalization of the Fermi velocity we need to compute the one-loop correction to the spatial component of the vertex

$$-iev\Gamma_1^i(k_1,k_2) = \int\frac{d^3k}{(2\pi)^3}(-ie\Gamma_0^0)iS_0(k_1+k)(-ie\Gamma_0^i)iS_0(k_2+k)(-ie\Gamma_0^0)iD_{0,00}(k). \tag{2.52}$$

In the same fashion as before we take the $k_1 = k_2 = 0$

$$-iev\Gamma_1^i = \frac{\mu^\epsilon ve^3\gamma^i}{2}\int\frac{d^{d-1}\mathbf{k}}{(2\pi)^{d-1}}\frac{d\omega_k}{2\pi}\frac{\omega_k^2+v^2\frac{3-d}{d-1}\mathbf{k}^2}{(\omega_k^2-v^2\mathbf{k}^2)(\omega_k^2-\mathbf{k}^2)^{1/2}}. \tag{2.53}$$

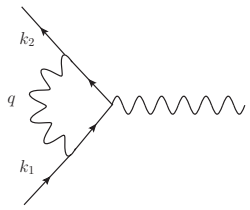

Figure 2.4: One-loop vertex correction.

The explicit dimensional factors in the numerator arise from manipulations of the γ matrices. We can immediately anticipate that this term is not UV divergent as it is proportional to ϵ, which promptly cancels with the usual ϵ^{-1} factor from the expansion of the Γ-function arising from the loop integral. We thus keep only the frequency term in the following. Performing first the frequenct integral

$$-iev\Gamma_1^i = -\frac{\mu^\epsilon e^3 v\gamma^i}{8\pi}\int_0^1 dx \frac{x}{\sqrt{1-x}(1-x(1-v^2))}\int \frac{d^{d-1}\mathbf{k}}{(2\pi)^{d-1}}\frac{1}{\mathbf{k}^2}. \tag{2.54}$$

Once again we skim over the infrared divergence directly into the UV divergent term

$$\Gamma_{1k}^{\text{UV}} = -\frac{e^2}{32\pi^2}\int_0^1 dx \frac{x}{\sqrt{1-x}(1-x(1-v^2))}, \tag{2.55}$$

which evaluates to

$$\Gamma_{1k}^{\text{UV}} = -\frac{e^2}{16\pi^2}\left(-\frac{1}{1-v^2}+\frac{\cos^{-1}(v)}{v(1-v^2)^{3/2}}\right). \tag{2.56}$$

Once again we find perfect match with (2.44b) from the self-energy computation. According to (2.19b) subtracting (2.51) from (2.56) furnishes an independent computation of the Fermi velocity renormalization

$$\delta Z_v = -\frac{\alpha_v}{4\pi}\left(\frac{3v}{1-v^2}-\frac{(1+2v^2)\cos^{-1}(v)}{(1-v^2)^{3/2}}\right). \tag{2.57}$$

in complete agreement with (2.46). This also concludes the test of the Ward Identity for the model.

These results are readily comparable to those of the existing literature, specially that of Vozmediano [100], which have been essentially reproduced. The only difference is an extra term proportional to v^2 in which comes from considering the full interaction vertex, that is, the terms proportional to $(-iev\Gamma_0^i)^2$ (schematically). These however do not significantly alter the fundamental features of the model. Just as pointed in [100, 101], the Fermi velocity renormalizes up until it reaches a fixed point at $v = c = 1$ in natural units. This is illustrated in figure 2.3.

Chapter 3

Reduced-Quantum Electrodynamics in curved space

We begin this chapter with a quick overview of curved spacetime quantum field theory. In particular we focus more heavily on the generalization to curved spacetimes of the spinorial quantities as this topic tends to be ignored on more introductory levels. Once again the goal is to lay down the conventions herein adopted and at the same time to keep the work self-contained. Standard introductory books to the subject include [50, 51].

3.1 Curved spacetime mathematics

The standard curved spacetime generalization is achieved by promoting the Minkowski metric to a general spacetime dependent metric $\eta_{\mu\nu} \to g_{\mu\nu}(x)$ and following the minimal coupling prescription for derivatives, i.e.

$$\partial_\mu V_\nu \to \nabla_\mu V_\nu = \partial_\mu V_\nu - \Gamma^\lambda{}_{\mu\nu} V_\lambda, \tag{3.1}$$

where $\Gamma^\lambda{}_{\mu\nu}$ is the Christoffel symbol defined from the metric as

$$\Gamma^\lambda{}_{\mu\nu} = \frac{1}{2} g^{\lambda\rho}(\partial_\mu g_{\lambda\nu} + \partial_\nu g_{\mu\lambda} - \partial_\lambda g_{\mu\nu}). \tag{3.2}$$

Notice that the Christoffel symbol is symmetric in the lower indices. For a contravariant vector V^μ the sign of the Christoffel symbol term in (3.1) is reversed. Covariant derivatives of tensors follow the appropriate recipe for every index separately, e.g., for a mixed tensor T^α_β

$$\partial_\mu T^\alpha_\beta \to \nabla_\mu T^\alpha_\beta = \partial_\mu T^\alpha_\beta - \Gamma^\alpha{}_{\mu\lambda} T^\lambda_\beta + \Gamma^\lambda{}_{\mu\beta} T^\alpha_\lambda. \tag{3.3}$$

The Riemann curvature tensor $R^\mu{}_{\nu\alpha\beta}$ is defined as

$$R^\mu{}_{\nu\alpha\beta} = \partial_\alpha \Gamma^\mu{}_{\nu\beta} - \partial_\beta \Gamma^\mu{}_{\nu\alpha} + \Gamma^\mu{}_{\alpha\rho}\Gamma^\rho{}_{\nu\beta} - \Gamma^\mu{}_{\beta\rho}\Gamma^\rho{}_{\nu\alpha}. \tag{3.4}$$

$R^\mu{}_{\nu\alpha\beta}$ enjoys some useful properties, such as anti-symmetry in $\alpha \leftrightarrow \beta$, as is evident from the definition, and also Bianchi's identity

$$R^\mu{}_{\nu\alpha\beta} + R^\mu{}_{\beta\nu\alpha} + R^\mu{}_{\alpha\beta\nu} = 0. \tag{3.5}$$

The completely covariant Riemman tensor $R_{\mu\nu\alpha\beta}$ is also antisymmetric in $\mu \leftrightarrow \nu$ and symmetry under the exchange of the pair of indices $(\mu\nu) \leftrightarrow (\alpha\beta)$. Tracing Riemman's curvature tensor once yields the Ricci tensor

$$R_{\alpha\beta} = R^\mu{}_{\alpha\mu\beta}, \tag{3.6}$$

which is always symmetric $R_{\alpha\beta} = R_{\beta\alpha}$. Finally one obtains the Ricci scalar by tracing the Ricci tensor

$$R = R^\alpha{}_\alpha. \tag{3.7}$$

We emphasize that every index contraction is done with the curved metric $g_{\mu\nu}$ or its inverse $g^{\mu\nu}$.

As mentioned back in section 1.4 it is possible to produce both curvature and torsion in the graphene layer. So far we have only discussed the formulae relating to curvature. This has been implicitly fixed by the symmetric Christoffel symbol in (3.2). When torsion is admitted $\Gamma^{\lambda}_{\ \mu\nu}$ acquires an anti-symmetric component in the two low indices. In this work however we will be looking only into curvature effects. The inclusion of torsion, and the most general curvature-torsion combination, is presently a natural open direction of development of the model we will briefly remark upon later.

Turning now to spinors we notice a different approach than that for vectors and tensors is needed to achieve coupling to curvature. The blatant practical reason being that the spinor's absence of spacetime indices render the usual algorithm inapplicable as it is. This problem is resolved by introducing at every point of the curved spacetime a locally flat Minkowskian frame with a local Lorentz invariant metric η_{ab}. Henceforth latin indices from the beginning of the alphabet will denote spacetime indices of the local frame. The link between the curved and flat spaces is encoded by the so-called vielbeins $e^{a}_{\ \mu}(x)$ through

$$g_{\mu\nu} = e^{a}_{\ \mu} e^{b}_{\ \nu} \eta_{ab}. \tag{3.8}$$

Operationally speakingthe vielbeins effectively transform local flat spacetime quantities into their curved spacetime analogs. In this fashion we can therefore define the curved spacetime γ-matrices as

$$\gamma^{\mu}(x) = e^{\mu}_{a}(x)\gamma^{a}, \tag{3.9}$$

where now γ^{a} are the standard flat space γ matrices obeying $\{\gamma^{a}, \gamma^{b}\} = 2\eta^{ab}$, whereas for γ^{μ} we get

$$\{\gamma^{\mu}, \gamma^{\nu}\} = 2g^{\mu\nu}. \tag{3.10}$$

Now it is possible to define the so-called spin connection

$$\omega_{\mu}^{\ a}{}_{b} = e_{b}^{\ \nu}(-\delta^{\lambda}_{\ \nu}\partial_{\mu} + \Gamma^{\lambda}_{\mu\nu})e^{a}_{\ \lambda}. \tag{3.11}$$

Then the curved space covariant derivative for spinors is written

$$\partial_{\mu}\psi \to \nabla_{\mu}\psi = \partial_{\mu}\psi + \frac{1}{8}\omega_{\mu}^{\ ab}\left[\gamma_{a}, \gamma_{b}\right]. \tag{3.12}$$

The covariant derivative of the vielbeins must vanish, a result known as the metricity condition

$$\nabla_{\mu}e^{a}_{\ \nu} = \partial_{\mu}e^{a}_{\ \nu} - \Gamma^{\lambda}_{\ \mu\nu}e^{a}_{\ \lambda} + (\omega_{\mu})^{a}_{\ b}e^{b}_{\ \nu} = 0. \tag{3.13}$$

Although unnecessary for our purposes, it is possible to completely rewrite every quantity and formulae exclusively in terms of the vielbeins.

The Dirac equation for graphene then takes the form

$$i\gamma^{\mu}(x)\nabla_{\mu}\psi = 0. \tag{3.14}$$

Already from this equation it has been shown [34] that smooth curvature in graphene sheets tend to decrease the Fermi velocity. The way it works is that v_F gets accompanied by a factor $\lambda \leq 1$ that depends exclusively on the geometry (equality holding for flat space). Notice this is an effect of the curvature alone and does not take into account interactions.

The last ingredient in the recipe concerns integrals over the spacetime volume, such as those appearing in the action. Volume integrals pick up a Jacobian factor from the non-trivial metric

$$\int d^{d}x \to \int d^{d}x\sqrt{-g}, \tag{3.15}$$

with $g = \det g_{\mu\nu}$ the metric determinant. This ensures the volume element is a scalar quantity and is therefore necessary to write down a meaningful action in curved spacetime.

3.2 On the curved space generalization of the PQED action

Armed with the tools just described it is we are ready to generalize the mixed QED action (2.1) for curved space. For the sake of generality we work in general mixed (d_{γ}, d_{e}) dimensions

$$S = \int d^{d_{\gamma}}x\sqrt{-g}\left[-\frac{1}{4}F_{\mu\nu}F^{\mu\nu} - \frac{1}{2\xi}(\nabla_{\mu}A^{\mu})\right] + \int d^{d_{e}}x\sqrt{-h}\bar{\psi}_{A}\, i\gamma^{\mu}(x)(\partial_{\mu} + \Omega_{\mu} + ieA_{\mu})\psi_{A}, \tag{3.16}$$

where $\Omega_\mu = (1/8)\omega_\mu{}^{ab}[\gamma_a, \gamma_b]$ is a commonly used shorthand convention for the spin connection term in the spinorial covariant derivative. Notice that the gauge field strength can still be written $F_{\mu\nu} = \partial_\mu A_\nu - \partial_\nu A_\mu$ without error, because of the Christoffel symbol terms cancel out due to their symmetry in the two low indices. Furthermore $h = -\det h_{\alpha\beta}$ is the induced metric on the boundary of the spacetime with metric $g_{\mu\nu}$. Besides the hypothesis of weak curvatures made in section 3.4, the formalism presented here can be elaborated without fixing a particular form to the metric. That said, for application to the specific case of graphene, one usually considers metrics in a normal Gaussian-coordinate form, that is (in four spacetime dimensions)

$$g_{\mu\nu}dx^\mu dx^\nu = dt^2 - dz^2 - h_{ij}dx^i dx^j. \tag{3.17}$$

This captures spatial defects only, which is precisely what we expect. However we must comment that it is also possible to effectively devise time curvature, see [Lewenkopf] where this is achieved within an external magnetic field. Finally since we don't expect the curvature-inducing graphene defects to be dynamical we refrain from including the Einstein-Hilbert action in the model.

Attempting the minimal coupling prescription directly on PQED action (2.10) is immediately met with the challenge of trying to make sense of the operator $(\nabla^\rho\nabla_\rho)^{-1/2}$. In flat PQED the non-local operator is promptly interpreted in the convolutional sense and momentum space methods were still applicable. In the curved case one is faced with the inverse of a complicated spacetime dependence in the metric through the Christoffel symbols within the covariant derivatives. Furthermore the PQED action (2.10) employs an effective gauge field designed to reproduce the appropriate behavior of QED's interactions. For this reason it is not obvious if an application of the minimal coupling to (2.10), if one even exists, would lead to an equivalent model as that in (3.16). For these reasons we do not make any attempt to tackle a curved space generalization of (2.10) in this work. Instead we will work with the curved mixed QED (3.16) and show that under appropriate conditions to be discussed a set of Feynman rules generalizing (2.9) exists and is just as easily employed for real computations.

To achieve this goal we follow a similar path as the one that lead us from mixed QED (2.1) to RQED (2.9). First we define

$$\bar{e}^a{}_\mu(x) = \begin{cases} e^a{}_\mu(x)\delta(x^{d_\gamma - d_e}) & a, \mu = \mu_e \\ 0 & a, \mu = d_e, \ldots, d_\gamma - 1. \end{cases} \tag{3.18}$$

This allows us to rewrite everything in the same dimension without spoiling the model in any way. The only difference from what was done in chapter 2 is that here we have used the vielbein in place of the current previously. In the case of graphene, $x^{d_\gamma - d_e} = z$, see Eq. (3.17). Moreover, we consider that the extra dimensions $d_\gamma - d_e$ are all flat which justifies the usage of the standard Dirac delta function. In this way the action displays a form which closely resembles the one of the standard QED in curved space, namely

$$S = \int d^{d_\gamma}x\sqrt{-g}\left[-\frac{1}{4}F_{\mu\nu}F^{\mu\nu} - \frac{1}{2\xi}(\nabla_\mu A^\mu) + \bar{\psi}_A\, i\bar{\gamma}^\mu(x)(\partial_\mu + \Omega_\mu + ieA_\mu)\psi_A\right] \tag{3.19}$$

where $\bar{\gamma}^\mu(x) = \bar{e}_a{}^\mu(x)\gamma^a$. Action (3.19) will be the starting point of our analysis. The next step is to integrate out the orthogonal degrees of freedom, but clearly this is not as straightforward as in a flat world. Luckily there exists some conditions that ultimately enable us to achieve this task that will be discussed later in section 3.4. Right now it is useful to make a parenthesis to go through the Ward Identity for curved space RQED.

3.3 Ward Identity for curved space RQED

Here we will quickly derive the Ward Identity within curved space RQED. Doing so at this point will establish the gauge invariance of the model from the get-go. This is useful because, as we will see, the Feynman rules for curved RQED will look like they violate gauge invariance, more specifically the gauge field propagator.

Consider the path-integral formulation of the theory, whose generating functional is given by

$$Z = \int DA_\mu D\psi D\bar{\psi}\exp\left\{iS + i\int d^{d_\gamma}x\sqrt{-g}\left(J^\mu A_\mu + \bar{\eta}\psi + \bar{\psi}\eta\right)\right\} \tag{3.20}$$

where S is given by (3.19). There should be also the contribution of the Faddeev-Popov ghost fields to the generating functional which is important in the evaluation of the one-loop effective action; since they will not play a role in our investigation, we choose to omit them for brevity.

Using functional methods, it is not difficult to exhibit the Schwinger-Dyson equation for the fermion propagator:

$$-iS^{-1}(x,x') = -iS_0^{-1}(x,x') + i\Sigma(x,x') \tag{3.21}$$

where S_0 is the free curved-space counterpart of the fermion propagator and the self-energy reads

$$-i\Sigma(x,x') = \int d^{d_\gamma}z\sqrt{-g(z)}\int d^{d_\gamma}u\sqrt{-g(u)}(-ie\gamma^\mu(x))iS(x,u)\big(-ie\Gamma^\nu(u,x';z)\big)iG_{\mu\nu}(z,x) \tag{3.22}$$

with $G_{\mu\nu}$ being the exact gauge propagator. In addition, $\Gamma^\nu(u,x';z)$ is the exact three-point function with the external exact propagator removed:

$$\Gamma^\nu(u,x';z) = \frac{\delta^3\Gamma}{\delta A_\nu(z)\delta\psi(u)\delta\bar{\psi}(x')} \tag{3.23}$$

where Γ is the proper vertex and the functional derivatives are taken with respect to the so-called classical fields. The inverse fermion propagator can also be given as

$$S^{-1}(x,x') = \frac{\delta^2\Gamma}{\delta\psi(x)\delta\bar{\psi}(x')}. \tag{3.24}$$

The derivation of the Schwinger-Dyson equation for the gauge propagator follows along similar lines; one finds

$$-iG^{-1}_{\mu\nu}(x,x') = -iG^{-1}_{0\mu\nu}(x,x') - i\Pi_{\mu\nu}(x,x') \tag{3.25}$$

where $G_{0\mu\nu}$ is the free gauge propagator in curved space. The vacuum polarization is defined as

$$i\Pi^{\mu\nu}(x,x') = -\int d^{d_\gamma}y\sqrt{-g(y)}\int d^{d_\gamma}y'\sqrt{-g(y')}\mathrm{Tr}\Big[(-ie\gamma^\mu(x))iS(x,y)\big(-ie\Gamma^\nu(y,y';x')\big)iS(y',x)\Big]. \tag{3.26}$$

The proof of the Ward-Takahashi identity for QED in curved space can be found in Ref. [110]. In the present case we can follow a similar procedure. Namely, let A_μ change by $\nabla_\mu\varphi(x)$. This amounts to consider a change in $\bar{\psi}$ and ψ,

$$\bar{\psi}(x) \to e^{-ie\,\varphi(x)}\bar{\psi}(x).$$

This implies the following change in $S^{-1}(x,x')$:

$$\delta S^{-1}(x,x') = e\int d^{d_\gamma}y\sqrt{-g(y)}\,\varphi(y)\nabla_\mu\Gamma^\mu(x,x';y). \tag{3.27}$$

But $\delta S^{-1}(x,x')$ can also be calculated from the transformation for in $\bar{\psi}$ and ψ, which gives

$$\delta S^{-1}(x,x') = ie\int d^{d_\gamma}y\sqrt{-g(y)}\,\varphi(y)[\delta(x,y)-\delta(x',y)]S^{-1}(x,x') \tag{3.28}$$

where $\delta(x,y) = (-g(y))^{-1/2}\delta^{d_\gamma}(x-y)$. Comparing both expressions, one arrives at the Ward-Takahashi identity

$$\nabla_\mu\Gamma^\mu(x,x';y) = i[\delta(x,y)-\delta(x',y)]S^{-1}(x,x'). \tag{3.29}$$

Simple usage of the definition of the vacuum polarization together with Eq. (3.29) leads us to the Ward identity in curved space:

$$\nabla^{x'}_\nu\,\Pi^{\mu\nu}(x,x') = 0. \tag{3.30}$$

This derivation was carried out for the model defined by the action (3.19). But since this is equivalent to the action given by Eq. (3.16), the validity of the Ward identity for RQED in curved space is hence established.

3.4 Local Momentum Space Representation

In this section we discuss momentum space versions for the curved photon and electron propagators in RQED. We employ two expansions, namely the Riemann normal coordinates (RNC) and the proper-time Schwinger-DeWitt expansion. Together they yield the local momentum space representation for the propagators. Due to the rather involved technical details we decide to focus mainly on the physical fundamentals of the approach, referring the details to the literature [50, 51]. Following the theme we start with QED$_4$, where results are already available, then proceed with the dimensional reduction to RQED.

3.4.1 QED$_4$

The starting point are the wave equations obeyed by the propagators $G^i{}_j(x,x')$ [109]

$$\left[\delta^i_k\Box + Q^i{}_k(x)\right]G^k{}_j(x,x') = \vartheta\delta^i_j\delta(x,x') \tag{3.31}$$

where the indices i,j indicate any appropriate indices carried by the fields of interest (spinor or vector), $\vartheta=+1$ for the gauge field and $\vartheta=-1$ for the spinor field. $Q^i{}_k(x)$ is a function with indices of the indicated type arising from manipulation of the covariant derivative (which acts on the x-dependence)

$$\nabla_\mu G^i{}_j(x,x') = \partial_\mu G^i{}_j(x,x') + \Gamma_\mu{}^i{}_k(x)G^k{}_j(x,x') \tag{3.32}$$

where $\Gamma_\mu{}^i{}_k$ is the appropriate connection for the given spin. It turns out that for the photon $Q_{\mu\nu}=R_{\mu\nu}$ and for the electron $Q^i{}_j=\delta^i{}_jR/4$, with i,j here spinor indices.

Let us first discuss the Riemann normal coordinates expansion. In simple terms it amounts to the application of the Equivalence Principle on some point x'. This allows a strictly flat spacetime description on x' where the standard methods of field theory are valid. For points within the normal neighborhood of x', defined as the region around x' where no geodesic crossings occur, we pick corrections that are polynomial in the curvature tensors and their derivatives computed at x'. For explicit expressions and further details see [50, 51].

The Schwinger-DeWitt expansion on the other hand is done directly on the fields' propagators. It makes use of the fact that $G(x,x')$ is a transition amplitude $\langle x,s|x',0\rangle$ evolving under a Schrödinger equation from proper time $\tau=0$ to $\tau=s$. For $x\to x'$ we fall into the domain of validity of the RNC expansion, which ultimately leads to the following fermionic and gauge propagators

$$\begin{aligned}
S_0(x,x') &= \int\frac{d^Dk}{(2\pi)^D}e^{-iky}\left[\frac{\gamma^\nu k_\nu}{k^2-M_e^2}+\frac{1}{(k^2-M_e^2)^2}\left(\frac{1}{2}R_{\nu\rho}\gamma^\nu k^\rho-\frac{\gamma^\nu k_\nu}{6}R\right)\right.\\
&+ \left.\frac{2}{3}\frac{\gamma^\nu k_\nu k^\sigma k^\rho R_{\rho\sigma}}{(k^2-M_e^2)^3}+\cdots\right]\\
D_{0\mu\nu'}(x,x') &= -\int\frac{d^{d_\gamma}k}{(2\pi)^{d_\gamma}}e^{-iky}\left[\frac{\eta_{\mu\nu'}}{k^2-M_\gamma^2}+\frac{1}{(k^2-M_\gamma^2)^2}\left(\frac{2}{3}R_{\mu\nu'}-\frac{1}{6}R\eta_{\mu\nu'}\right)\right.\\
&- \left.\frac{2}{3}\frac{(2R_{\mu\alpha\beta\nu'}-R_{\alpha\beta}\eta_{\mu\nu'})k^\alpha k^\beta}{(k^2-M_\gamma^2)^3}+\cdots\right].
\end{aligned}\tag{3.33}$$

In the above $M_e^2=R(x')/12$ and $M_\gamma^2=-R(x')/6$ are the result of a non-perturbative ressumation. Some comments are in order. First notice that $R(x')$ being computed at x' is formally a number. Furthermore since this is a semiclassical approximation neither M_e^2 nor M_γ^2 are subject to renormalization. Finally we must be careful before interpreting the poles at M_e^2 and M_γ^2 as physical masses because for a generic curved spacetime there is no unambiguous split between positive and negative frequencies to define one-particle states. For instance our general proof of the Ward Identity guarantees that there is no conflict between the parameter M_γ and gauge invariance.

Obviously, the local-momentum space representation provides only a local approximation to the propagator. However, it should give reasonable approximate results as long as curvature effects remain weak. It is in this sense that the expression for the optical conductivity to be calculated later on is to be regarded as a high-frequency expansion.

3.4.2 Reduced QED

Up until now our discussion parallels the one for standard curved QED$_4$. We still need to reduce the gauge sector down to $(2+1)$ dimensions. This is a difficult task for a general curved spacetime, but within the regime of validity of the local momentum space representation it can be done in the exact same fashion as in the flat spacetime case. We find to first order in the Feynman gauge

$$D_{0\mu\nu'}(k^2)=\frac{-i\eta_{\mu\nu'}}{2(k^2-M_\gamma^2)^{1/2}}. \tag{3.34}$$

This is the propagator we shall employ in the following one-loop analysis.

In a general gauge the gauge field propagator in QED_4 is to first order in the local momentum space representation

$$D_{0\mu\nu'}(k^2) = \frac{-i}{k^2 - M_\gamma^2}\left[\eta_{\mu\nu'} - (1-\xi)\frac{k_\mu k_{\nu'}}{k^2 - M_\gamma^2}\right]. \tag{3.35}$$

Within this approximation we find upon projection

$$D_{0\mu\nu'}(k^2) = \frac{-i}{(k^2 - M_\gamma^2)^{1/2}}\left[\eta_{\mu\nu'} - (1-\tilde{\xi})\frac{k_\mu k_{\nu'}}{k^2 - M_\gamma^2}\right]. \tag{3.36}$$

The above propagator seems to violate gauge invariance at first glance. The presence of M_γ inside the square brackets completely spoils the transversality of the propagator

$$k^\mu D_{0\mu\nu} = -i\frac{\tilde{\xi}k^2 - M_\gamma^2}{(k^2 - M_\gamma^2)^{3/2}}k^\nu \neq 0. \tag{3.37}$$

This is precisely what was alluded to when we set to prove the Ward Identity. So what is going on? We must remember that the $M_\gamma^2 = -R/6$ is next-to-leading order in the LMSR, whereas propagator (3.35) and consequently (3.36) are only of leading order in (3.33). The other offending term $\tilde{\xi}k^2$ is just the usual gauge dependent-term. Therefore it follows that (3.36) is indeed transversal and gauge invariant at leading order in the LMSR.

It is not straightforward, if possible at all, to infer a purely (2+1)-dimensional action that reproduces (3.36) in analogy to the passage from (2.9) to (2.10) - i.e. a curved space generalization to PQED. Furthermore, if indeed possible this would only be an UV limit of curved PQED. Finally we notice this is the reason for choosing the name curved RQED instead of curved PQED for the approach we adopt in this work.

3.5 One-Loop Analysis

We are now ready to compute the one-loop diagrams. In curved space the one-loop functions are written

$$\begin{aligned}
i\Pi_1^{\mu\nu}(x,x') &= -\mathrm{Tr}\Big[(-ie\gamma^\mu(x))iS_0(x,x')(-ie\gamma^\nu(x'))iS_0(x',x)\Big] \\
-i\Sigma_1(x,x') &= (-ie\gamma^\mu(x))iS_0(x,x')(-ie\gamma^\nu(x'))iD_{0\mu\nu}(x',x) \\
-ie\Gamma^\mu(y,y';x) &= (-ie\gamma^\beta(x))iS_0(x,y)(-ie\gamma^\mu(y))iS_0(x,y')(-ie\gamma^\alpha(y'))iD_{0\alpha\beta}(y',y)
\end{aligned} \tag{3.38}$$

These diagrams have the same UV divergences as their flat space counterparts. This is easily understood from the highly local nature of high energies. A theorem proved by Collins states that all counterterms are necessarily local in a flat background [111]. An important consequence of this theorem is that a non-local contribution in the action does not get renormalized (i.e., the associated $\delta Z = 0$). In the case of RQED in flat space, this implies that the beta function is zero to all orders in perturbation theory, producing thereby an explicit example of an interacting boundary conformal field theory. On the other hand, in a general curved space, by combining the local-momentum representation and the usual Feynman technique, one obtains that the necessary counterterms should also be covariant local expressions. This suggests that the beta function of curved-space RQED should also be zero to all orders in perturbation theory. The one-loop proof of this statement will be given in due course.

Although the actual computation of the divergences will greatly benefit from the LMSR it might still not be obvious how renormalization works out along the intricate technicalities of curved space. For this reason we will illustrate how renormalization goes for the one-loop fermion propagator in more detail at the expense of being a bit repetitive. For the complete story for quantum electrodynamics see [110].

The one-loop fermion propagator is given by

$$iS(x,x') = iS_0(x,x') + \int d^{d_\gamma}z\sqrt{-g(z)}\int d^{d_\gamma}z'\sqrt{-g(z')}iS_0(x,z)\big(-i\Sigma_1(z,z')\big)iS_0(z',x'). \tag{3.39}$$

In the spirit of generality this time we follow Teber [44] in keeping the dimension d_γ for the photon general. Loop integrals will depend on d_e which is given as a function of suitable quantities ϵ_γ and ϵ_e:

$$d_e = 4 - 2\epsilon_\gamma - 2\epsilon_e.$$

After evaluating the loop integrals for a general d_e, we employ the above expression for a fixed value of ϵ_e, namely $\epsilon_e = 1/2$. The associated divergences will correspond to poles in $1/\epsilon_\gamma$. The relation between bare and renormalized quantities follows the usual recipe (2.14).

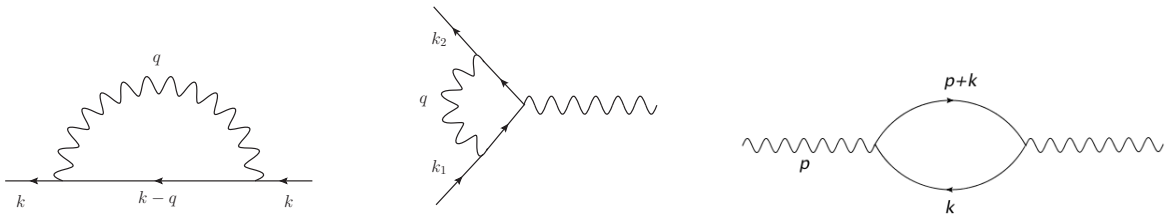

(a) One-loop fermion Self-Energy. (b) One-loop vertex correction. (c) One-loop vacuum polarization.

Figure 3.1: One-loop diagrams.

3.5.1 One-loop fermion Self-Energy

Now we turn to the task of studying the one-loop diagrams in detail. We start our discussion with the fermion self-energy. This is given by the second expression in Eq. (3.38), see also Fig. 3.1a. Considering Riemann normal coordinates with origin at x', one must insert into such an expression the fermion propagator in (3.33) and the photon propagator (3.36). One finds the following local-momentum representation for the one-loop fermionic self-energy:

$$\Sigma_1(k,x') = \frac{1}{2}\int \frac{d^3q}{(2\pi)^3}(-ie\gamma^\mu)\frac{i(\not{k}-\not{q})}{(k-q)^2-M_e^2+i\epsilon}(-ie\gamma^\nu)\frac{i\eta_{\mu\nu}}{(q^2-M_\gamma^2+i\epsilon)^{1/2}}. \tag{3.40}$$

As is clear from the above expression, we are working in the Feynman gauge, $\xi = 1$. Moreover, notice that we kept only the leading-order terms in the expansion in curvatures for the propagators. These are the only ones that will generate a divergence at $d_e = 3$ and hence to a $\tilde{\mu}$ dependence. Accordingly, we also kept only the leading-order term in the expansion of the gamma matrices, so the γ's in the above equation are just the standard flat-space gamma matrices in three dimensions.

Using that $\gamma^\mu\gamma^\alpha\gamma_\mu = -\gamma^\alpha$ and introducing standard Feynman parameters, one obtains

$$\Sigma_1(k,x') = \frac{e^2\not{k}}{16\pi^2}\int_0^1 du\sqrt{1-u}\left[\frac{1}{\bar{\epsilon}_\gamma} - \ln\left(\frac{\Delta - i\epsilon}{\mu^2}\right)\right] \tag{3.41}$$

where

$$\frac{1}{\bar{\epsilon}_\gamma} \equiv \frac{1}{\epsilon_\gamma} - \gamma_E + \ln 4\pi, \tag{3.42}$$

γ_E is Euler's constant and $\Delta = uM_e^2 + (1-u)M_\gamma^2 - u(1-u)k^2$.

Now let us present an explicit expression for the renormalization constant Z_2. Consider Eq. (3.39). Let us employ Riemann normal coordinates with origin at x'. In general, the expansions for $S_0(x,z)$ and $\Sigma_1(z,z')$ will be different from the expressions given previously since it is x' that is fixed and the arguments of such quantities do not contain x'. Then one should consider for $S_0(x,z)$ and $\Sigma_1(z,z')$ a more general momentum-space representation [112]. Nevertheless, at leading order the results are the same. Therefore, one finds the following one-loop local-momentum representation at leading order in the expansion in curvatures

$$S(k,x') = S_0(k,x') + S_0(k,x')\Sigma_1(k,x')S_0(k,x'). \tag{3.43}$$

Now consider the leading term in the expansion of $S_0(k,x')$. Since curvature effects are supposed to be sufficiently small, this can also be written as

$$S_{0,\text{leading}}(k,x') = \frac{\gamma^\nu k_\nu}{k^2-M_e^2} = \frac{\gamma^\nu k_\nu}{k^2} + \frac{\gamma^\nu k_\nu}{k^4}\frac{R(x')}{12} + \cdots \tag{3.44}$$

in other words, we obtain the standard local-momentum representation. Then Eq. (3.43) can be written as

$$iS(k,x') = \frac{i}{\not{k}} + \frac{i}{\not{k}}\left[-i\Sigma_1(k,x')\right]\frac{i}{\not{k}} + \cdots \tag{3.45}$$

where we are focusing only on the first term in the expansion for S_0 since this is the one important in discussing the renormalization. On the other hand, since $\psi = Z_2^{1/2}\psi_R$, one obtains that $S = Z_2 S_R$. Thus the

counterterm Lagrangian density will produce the following local-momentum representation for the fermionic propagator (at leading order)

$$iS_R(k,x') = \frac{i}{\not k} + \frac{i}{\not k}\left[i\delta Z_2^{(1)}\not k\right]\frac{i}{\not k} + \text{loops} + \cdots \tag{3.46}$$

where $\delta Z_2^{(1)}$ is the one-loop counterterm. Hence, adding the one-loop contribution calculated from Eq. (3.45) to Eq. (3.46), one obtains that

$$iS_R(k,x') = \frac{i}{\not k} + \frac{i}{\not k}\Big[-i\big(\Sigma_1(k,x') - \delta Z_2^{(1)}\not k\big)\Big]\frac{i}{\not k} + \mathcal{O}(\alpha^2) \tag{3.47}$$

at leading order in the expansion in curvatures. One can choose $\delta Z_2^{(1)}$ in such a way to cancel the divergence in $\Sigma_1(k,x')$. In this way one finally obtains

$$Z_2 = 1 + \frac{2}{3}\frac{\alpha_R}{4\pi\bar{\epsilon}_\gamma} + \mathcal{O}(\alpha^2) \tag{3.48}$$

where we have replaced α by α_R in such an expression (this is correct to leading order). This has the same form as in flat space [44]. Observe also that renormalization constant Z_2 at one-loop is unaffected by spacetime curvature, a result similar to the standard quantum electrodynamics in curved spacetime [110]. Curvature terms only contribute to the finite part of the self-energy:

$$\Sigma_{1\text{F}}(k,x') = -\frac{e^2\not k}{16\pi^2}\int_0^1 du\sqrt{1-u}\ln\left(\frac{\Delta - i\epsilon}{\mu^2}\right) \tag{3.49}$$

3.5.2 One-loop vertex correction

Let us now we turn our attentions to the vertex correction at one-loop order. This is given by the third expression in Eq. (3.38), see Fig. 3.1b. Again considering Riemann normal coordinates with origin at x', one must insert into such an expression the fermion propagator in (3.33) and the gauge propagator (3.36). By taking into account only the leading-order term of such an expansion, one finds that

$$e\Gamma_1^\mu(k_1,k_2,x') = \frac{1}{2}\int\frac{d^3q}{(2\pi)^3}\frac{i\eta_{\alpha\beta}}{(q^2-M_\gamma^2+i\epsilon)^{1/2}}(-ie\gamma^\beta)\frac{i(\not k_1+\not q)}{(k_1+q)^2-M_e^2+i\epsilon}(-ie\gamma^\mu)\frac{i(\not k_2+\not q)}{(k_2+q)^2-M_e^2+i\epsilon}(-ie\gamma^\alpha) \tag{3.50}$$

where as above we have considered the reduced gauge propagator in the Feynman gauge. The UV divergence is produced solely by the q^2 term, which is physically interpreted as a contribution to the charge form factor. So let us compute the vertex function for $k_1 = k_2 = 0$. Again following the standard procedure, one has that

$$\widetilde{\Gamma}_1^\mu(x') = \frac{e^2}{32\pi^2}\int_0^1 dydz\frac{\theta(-y-z+1)\theta(y+z)}{\sqrt{1-y-z}}\left[\frac{1}{\bar{\epsilon}_\gamma} - \frac{2}{3} - \ln\left(\frac{\widetilde{\Delta}-i\epsilon}{\tilde{\mu}^2}\right)\right]\gamma^\mu, \tag{3.51}$$

where $\widetilde{\Delta} = (1-y-z)M_\gamma^2 + (y+z)M_e^2$.

Now we must discuss the one-loop renormalization of the vertex function. This amounts to calculate the renormalization constant Z_1 at one-loop level. Proceeding as in the previous section, the vertex function up to one-loop level in the local-momentum representation can be written as

$$-ie\Gamma^\mu(k_1,k_2,x') = -ie\gamma^\mu - ie\Gamma_1^\mu(k_1,k_2,x') \tag{3.52}$$

where as above we considered only the leading order in the expansion in curvatures. On the other hand, the renormalized vertex function Γ_R^μ is given in terms of the associated bare quantity Γ^μ and Z_1 as

$$\Gamma_R^\mu(k_1,k_2,x') = Z_1^{-1}\Gamma^\mu(k_1,k_2,x') \tag{3.53}$$

again in leading order in the expansion in curvatures. The standard renormalization procedures then yields

$$Z_1 = 1 + \frac{2}{3}\frac{\alpha_R}{4\pi\bar{\epsilon}_\gamma} + \mathcal{O}(\alpha^2). \tag{3.54}$$

where as above we have replaced α by α_R. A simple comparison between Eqs. (3.54) and (3.48) shows that $Z_1 = Z_2$. So we have explicitly verified the constraint between such renormalization constants at one-loop order: This result, which is a consequence of the Ward-Takahashi identity, is still valid for the curved-space version of RQED.

3.5.3 One-loop vacuum polarization

Finally let us discuss the one-loop vacuum polarization. This is given by the first expression in Eq. (3.38). See also Fig. 3.1c. Again considering Riemann normal coordinates with origin at x', one must insert into such an expression the fermion propagator in (3.33) and the photon propagator (3.36). By taking into account only the leading-order term of such an expansion, one finds that

$$i\Pi_1^{\mu\nu}(p,x') = -e^2 \int \frac{d^3k}{(2\pi)^3} \mathrm{Tr}[\gamma^\mu\gamma^\alpha\gamma^\nu\gamma^\beta] \frac{(p+k)_\alpha k_\beta}{((p+k)^2 - M_e^2 + i\epsilon)(k^2 - M_e^2 + i\epsilon)}. \tag{3.55}$$

As above, in such an equation use is made of the flat-space version of the gamma matrices. Using properties of the traces of products of gamma matrices and introducing Feynman parameters, one finds the finite result

$$i\Pi_1^{\mu\nu}(p,x') = -\frac{ie^2}{2\pi}(p^2\eta^{\mu\nu} - p^\mu p^\nu) \int_0^1 dx \, \frac{x(1-x)}{\sqrt{M_e^2 - i\epsilon - x(1-x)p^2}} + \frac{ie^2 M_e^2}{4\pi}\eta^{\mu\nu} \int_0^1 dx \frac{1}{\sqrt{M_e^2 - i\epsilon - x(1-x)p^2}}. \tag{3.56}$$

Apparently the Ward identity is violated by the presence of an anomalous contribution, given by the second term on the right-hand side of the above equation. However, by evaluating the x-integrals one finds that the transversality breaking term is actually longitudinal; more importantly, since the numerator is proportional to $M_e^2 = R(x')/12$, such a term is of higher order in the curvature expansion currently considered. Thus at leading order

$$i\Pi_1^{\mu\nu}(p,x') = \frac{ie^2}{4\pi}(p^2\eta^{\mu\nu} - p^\mu p^\nu) \left[\frac{\sqrt{M_e^2 - i\epsilon}}{p^2} + \frac{1}{4p} \ln\left(\frac{2\sqrt{M_e^2 - i\epsilon} - p}{2\sqrt{M_e^2 - i\epsilon} + p} \right) \right] \tag{3.57}$$

and the Ward identity at one-loop order is satisfied.

The most relevant upshot from this calculation is that the vacuum polarization is finite, at least at one-loop order. This means that such a contribution does not get renormalized, $\delta Z_3^{(1)} = 0$. This in turn implies that the beta function of the curved-space version of RQED is zero at one-loop order.

3.6 Application to curved graphene layer

In this section we describe how to apply the formalism developed so far to the case of graphene. There are two small modifications to be made. First of all photons, contrary to electrons, are not subjected to a curved space. Therefore we set $M_\gamma^2 = 0$. Notice however that the one-loop vacuum polarization (3.57) is not affected by M_γ^2 as there are no internal gauge field propagators. Importantly the Ward Identity still holds for $M_\gamma^2 = 0$ as only a few immaterial factors of $|g|^{1/2}$ drop out. This is confirmed by the recovery of the known UV divergences from flat graphene, see from [101]. Secondly we must substitute γ^i by $v_F\gamma^i$, with $v_F \approx 1/300$. This takes into account the actual Fermi velocity of the Dirac excitations.

The Feynman rules for the application of the theory to graphene for the case of retarded Coulomb interaction produce the following expressions for the fermionic and gauge-field propagator, and the photon-fermion-fermion vertex, respectively:

$$\begin{aligned} iS_0(\omega_p, \mathbf{p}) &= \tfrac{i(\gamma^0\omega_p - v_F\gamma^i p^i)}{\omega_p^2 - v_F^2\mathbf{p}^2 - M_e^2 v_F^4} \\ iD_0(\omega_p, \mathbf{p}) &= \tfrac{1}{2}\tfrac{i}{\sqrt{-\omega_p^2 + \mathbf{p}^2}} \\ -ie\Gamma_0^0 &= -ie\gamma^0. \end{aligned} \tag{3.58}$$

The free fermion propagator above has the feature that it does not modify the density of states at x' because $M_e^2(x')$ is a momentum-independent constant within our framework. This readily follows from a similar computation as in (2.25)

$$\rho(\omega) = -\frac{1}{\pi}\mathrm{Im} \int d^2\mathbf{k} \, \mathrm{Tr} \left[\frac{\gamma^0\omega - v_F\boldsymbol{\gamma}.\mathbf{k}}{(\omega + i\epsilon)^2 - v_F^2\mathbf{k}^2 - M_e^2 v_F^4} \gamma^0 \right] = \frac{\omega}{2\pi v_F^2}, \tag{3.59}$$

where the $M_e^2 v_F^4$ term fails to contribute because the Jacobian from polar coordinates cancels with a scale factor from the delta function $\delta(\omega^2 - v_F^2 k^2 - M_e^2 v_F^4)$ after integration, leading to the usual linear ω/v_F^2 behavior around the Dirac points. Therefore a gap does not open.

3.6.1 1-loop fermion self-energy

Let us discuss the one-loop self-energy. One finds that

$$-i\Sigma_1(\omega_p,\mathbf{p}) = \frac{e^2}{2}\int \frac{d^{d-1}\mathbf{k}}{(2\pi)^{d-1}}\frac{d\omega_k}{2\pi}\frac{\gamma^0(\gamma^0(\omega_k+\omega_p)-v_F\gamma^i(k+p)_i)\gamma^0}{((\omega_k+\omega_p)^2-v_F^2(\mathbf{k}+\mathbf{p})^2-M_e^2v_F^4)(\omega_k^2-\mathbf{k}^2)^{1/2}}. \tag{3.60}$$

Having already established that the UV divergences are in general the same as in the flat model, we just state the result for the Fermi velocity renormalization

$$\delta Z_v = -\frac{\alpha_g}{4\pi}\left(\frac{3}{1-v_F^2}-\frac{(1+2v_F^2)\cos^{-1}v_F}{v_F(1-v_F^2)^{3/2}}\right), \tag{3.61}$$

which, apart from a constant factor proportional to the square of the Fermi velocity (coming from the current density interaction of the vertex we have dropped), we recover the results from Ref. [100], which we refer for further details. The beta function β_v is shown in Fig. 2.3. The crucial point here is that, according to our model, the relativistic fixed point achieved for $v_F \to 1$ is predicted to survive in the presence of disclination-induced curvature.

As for the finite part of the self energy, we are particularly interested in the imaginary part of Σ_1^F as it translates to the scattering time among the charge carriers in graphene due to the electromagnetic interaction in the presence of curvature. The local $\mathbf{p}\to 0$ limit is relevant when considering level-broadening effects on the conductivity

$$\Sigma_1^F(\omega_p) = -\frac{\alpha_g}{4\pi}\gamma^0\omega_p\int_0^1 dx\frac{\sqrt{1-x}}{1-x(1-v_F^2)}\log\left(\frac{\bar{\mu}^2}{x\left(M_e^2v_F^4-(1-x)\omega_p^2\right)-i\epsilon}\right) \tag{3.62}$$

There are now two possible cases to consider, namely positive or negative Ricci scalar. For positive Ricci scalar, i.e. $M_e^2>0$, we obtain, for the scattering time:

$$\tau_+^{-1}(z) = \frac{\alpha_g}{4}M_ev_F^2z\int_0^1 dx\frac{\sqrt{1-x}}{1-x(1-v_F^2)}\theta((1-x)z^2-1), \tag{3.63}$$

where $z^2=\omega_p^2/M_e^2v_F^4$. This integrates to

$$\tau_+^{-1}(z) = \begin{cases} 0, & z<1 \\ \frac{\alpha_g}{4}M_ev_F^2z\left(\frac{2}{1-v_F^2}\left(1-\frac{1}{z}\right)+\frac{2}{(1-v_F^2)^{3/2}}\left(\cot^{-1}\left(\frac{v_Fz}{\sqrt{1-v_F^2}}\right)-\cos^{-1}v_F\right)\right), & z>1. \end{cases} \tag{3.64}$$

For negative Ricci scalar, i.e. $M_e^2<0$, the self-energy always acquires an imaginary part. In this case, the scattering time is given by

$$\tau_-^{-1}(z) = \frac{\alpha_g}{4}M_ev_F^2z\left(\frac{2}{1-v_F^2}-\frac{2v_F\cos^{-1}v_F}{(1-v_F^2)^{3/2}}\right). \tag{3.65}$$

3.6.2 1-loop vertex correction

Now let us consider the one-loop vertex correction at zero external momenta. This is given by

$$-ie\Gamma_1^\mu(0,0) = \frac{e^3}{2}\int\frac{d^{d-1}\mathbf{k}}{(2\pi)^{d-1}}\frac{d\omega_k}{2\pi}\frac{\gamma^0\gamma^\alpha\gamma^\mu\gamma^\beta\gamma^0k_\alpha k_\beta}{(\omega_k^2-v_F^2\mathbf{k}^2)^2(-\omega_k^2+\mathbf{k}^2)^{1/2}}. \tag{3.66}$$

It is straightforward to verify that the UV divergences match those of $-i\Sigma_1$. We once more refer to [100] for further details. The finite parts of the time and spatial components read

$$\Gamma_1^{0,F}\gamma^0 = -\frac{\alpha\gamma^0}{8\pi}\int_0^1 dx\frac{x}{\sqrt{1-x}}\left(\frac{1}{1-x(1-v_F^2)}-\frac{2v_F^2}{(1-x(1-v_F^2))^2}\right)\log\left(\frac{(1-x(1-v_F^2))\bar{\mu}^2}{xM_e^2v_F^4}\right), \tag{3.67}$$

and

$$v_F\Gamma_1^{i,F}\gamma^i = -\frac{\alpha v_F\gamma^i}{8\pi}\int_0^1 dx\frac{x}{\sqrt{1-x}}\left(\frac{1}{1-x(1-v_F^2)}\log\left(\frac{(1-x(1-v_F^2))\bar{\mu}^2}{xM_e^2v_F^4}\right)+\frac{v_F^2}{(1-x(1-v_F^2)^2}\right). \tag{3.68}$$

These allow us to define a suitable effective Fermi velocity:

$$\frac{1}{v_{\text{eff}}} = \frac{1}{v_F}\left(1 + \frac{(\Gamma_1^{0,F})^3}{\Gamma_1^{i,F}}\right). \tag{3.69}$$

Fixing $\bar{\mu}^2 = M_e^2 v_F^4$ the correction leads to a higher effective Fermi velocity in accordance with expectation from the running in figure 2.3

$$v_{\text{eff}} \approx 1.0072 v_F. \tag{3.70}$$

In Ref. [34] it was shown that the curvature has the effect of decreasing the Fermi velocity. On the other hand, electron-electron interactions tend to increase the Fermi velocity. Eq. (3.70) shows that the impact of electron-electron interactions is stronger than that of the curvature.

3.6.3 Higher-frequency behavior of the optical conductivity

As an application of the above results, let us determine the high-frequency behavior of the optical conductivity in the presence of curvature effects in graphene by using the Kubo formula, which describes the linear response to a static external electric field. In real time, it is given by

$$\sigma^{ik} = \lim_{\mathbf{p}\to 0} i\frac{\langle j^i j^k\rangle}{\omega + i\epsilon} \tag{3.71}$$

where the current correlation function is meant to contain only one-particle irreducible (1PI) diagrams. A simple analysis shows that [43]

$$\langle j_\mu j_\nu\rangle_{1\text{PI}} = \Pi_{\mu\nu} \tag{3.72}$$

where $\Pi_{\mu\nu}$ is the vacuum polarization tensor of the electromagnetic field. The optical conductivity is then given by

$$\sigma^{jk}(\omega) = \lim_{\mathbf{p}\to 0} \frac{i\Pi^{jk}}{\omega + i\epsilon}. \tag{3.73}$$

To derive the optical conductivity from the above formula, one must change the boundary conditions employed so far. This amounts to considering the various Green functions appearing in Eq. (3.38) with retarded boundary conditions. In this case the loop integrals in the vacuum polarization are to be calculated using the in-in formalism, see for instance Ref. [113]. The result has the same functional dependence, but with a different $i\epsilon$ prescription:

$$q^0 \to q^0 + i\epsilon.$$

The one-loop vacuum polarization is then given by

$$i\Pi_1^{\mu\nu}(p,x') = \frac{ie^2}{4\pi}(p^2\eta^{\mu\nu} - p^\mu p^\nu)\left[\frac{\sqrt{M_e^2 v_F^4}}{p^2} + \frac{1}{4p}\ln\left(\frac{2\sqrt{M_e^2 v_F^4} - p}{2\sqrt{M_e^2 v_F^4} + p}\right)\right], \quad p^\mu = (p^0 + i\epsilon, \mathbf{p}). \tag{3.74}$$

Geometrically it is perfectly plausible for M_e^2 to be either negative or positive. Both possibilities seem to lead to qualitatively different behavior due to extra factors of i arising for $M_e^2 < 0$. In the following we will focus mostly on the positive scalar-curvature case where the physics is clearer, and we give only a brief discussion on the negative case at the end of this section. With that in mind, we combine our results to obtain the high-frequency behavior of the optical conductivity:

$$\sigma^{jk}(z,x') = \frac{e^2}{4}\left[\frac{4}{\pi}\frac{i}{z+i\epsilon} + 1 + \frac{i}{\pi}\ln\left(\frac{z+i\epsilon-2}{z+i\epsilon+2}\right)\right]\eta^{jk}. \tag{3.75}$$

Observe that σ^{jk} a function of the ratio $z = \omega/\sqrt{M_e^2 v_F^4}$. The conductivity for the case $M_e^2 > 0$ is depicted in Fig. 3.2a. A similar result was obtained in [114] which we reproduce here for convenience for zero temperature and mass gap but finite chemical potential in the local limit, suggesting a chemical potential interpretation of $\sqrt{M_e^2}$. In this way we can understand the first term as due to intraband transitions, and the remaining as the interband contribution. The latter is just the minimal graphene conductivity $\sigma_0 = e^2/4$ for $z > 2\sqrt{M_e^2}$. The absence of interband transitions for $z < 2\sqrt{M_e^2}$ is due to the kinematics of momentum conservation of

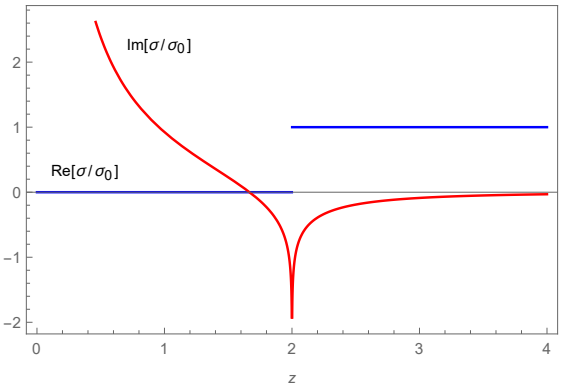

(a) Real and imaginary parts of $\sigma^{jj}(z, x')$ normalized to σ_0 without broadening effects.

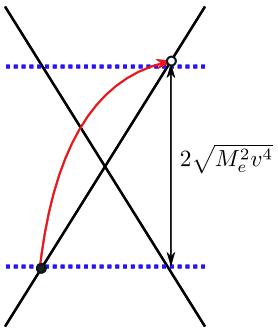

(b) Origin of conductivity jump under a finite chemical potential (blue line).

Figure 3.2: Non-interacting conductivity in graphene with a finite chemical potential.

chiral fermions as illustrated in Fig. 3.2b. Even though the validity of the local momentum representation translates to high-frequency regime, our result seems to work for all z given the identification $\sqrt{M_e^2} = \mu$.

If one wishes to include curvature effects of level broadening due to scattering of the fermion, then one should replace $i\epsilon$ by $\tau_+^{-1}(z)$ in the expression of the optical conductivity. One obtains

$$\sigma^{jk}(z, x') = \frac{e^2}{4}\left[\frac{4}{\pi}\frac{i}{z + i\tau_+^{-1}(z)} + 1 + \frac{i}{\pi}\ln\left(\frac{z + i\tau_+^{-1}(z) - 2}{z + i\tau_+^{-1}(z) + 2}\right)\right]\eta^{jk}. \tag{3.76}$$

If $\mathrm{Im}[\Sigma_1^F(\omega)]$ is small, we can approximate it as a constant value, which results in a constant τ_+^{-1}. This implies that in this case this expression can also be obtained by employing resummed fermionic propagators in the calculation of the vacuum polarization. The result will resemble a simple one-loop calculation, even though higher-order corrections are being taken into account with the usage of dressed propagators. This is somewhat reminiscent of the standard discussion on unstable particles in high-energy scattering amplitudes within the narrow-width approximation. In the context of condensed-matter settings, a vanishingly small imaginary part of the self-energy (around the Fermi surface) implies that the criterion for the Fermi-Landau liquid theory is fully justified.

Let us first consider the full frequency dependence of τ_+^{-1}. When $M_e^2 > 0$ we see from Fig. 3.3 that there is no longer a jump on the real part of the conductivity at $z = 2$. Instead, the conductivity starts to increase smoothly at $z = 1$. Accordingly the imaginary part of $\sigma(z)$ is also smoothened at $z = 2$, as dictated by the Kramers-Kronig relations. For $z \to \infty$ we still recover σ_0. Eq. (3.76) is similar to the one found in Ref. [115], except for the fact that here the scattering time given by Eq. (3.64) kicks in only at $z = 1$.

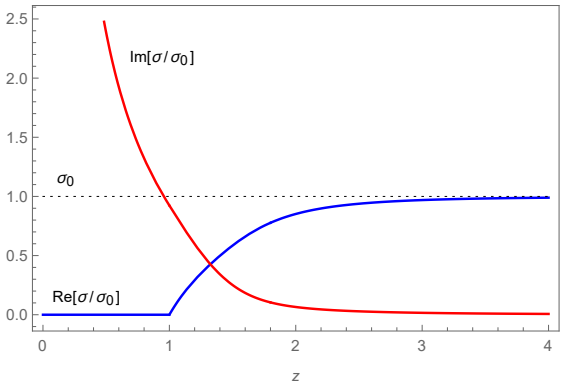

Figure 3.3: Real and imaginary parts of optical conductivity normalized to σ_0 with broadening effects for positive Ricci curvature scalar. Dotted line shows that the minimum conductivity σ_0 is approached asymptotically.

One may consider the conductivity for a fixed value of τ_+^{-1}, somewhat partially similar to what was undertaken in Ref. [115]. We explore this situation for the case in which $\mathrm{Im}[\Sigma_1^F(\omega)]$ is small so that τ_+^{-1} can be taken to be approximately constant. This will take place near the Fermi energy. In fact, just above the Fermi energy the imaginary part of the self energy with $\mathbf{p} = 0$ obeys a linear relationship with ω_p, indicating that the (undoped) graphene behaves as a marginal Fermi liquid – a result consistent with the conclusions of Ref. [116]. As an illustration, let us quote our result for a matching scale of $z = z_0$, $z_0 \gtrsim 1$, for the scattering time (Fermi energy amounts to choosing $z_0 = 1$):

$$\sigma^{jk}(z, x') = \frac{e^2}{4}\left[\frac{4}{\pi}\frac{i}{z + i\tau_+^{-1}(z_0)} + 1 + \frac{i}{\pi}\ln\left(\frac{z + i\tau_+^{-1}(z_0) - 2}{z + i\tau_+^{-1}(z_0) + 2}\right)\right]\eta^{jk}. \tag{3.77}$$

It is easy to see that there is an enhancement in the minimal conductivity for $z \geq 2$:

$$\sigma_0 \to \sigma_0 + \frac{e^2}{\pi}\frac{\tau_+^{-1}(z_0)}{z^2 + \tau_+^{-2}(z_0)}. \tag{3.78}$$

For $z < 2$ the intraband contribution produces a positive contribution to the real part of the optical conductivity, whereas the log yields a (constant) negative contribution. However, for $z \to 0$, the intraband transition is the dominant term, and a positive contribution remains. In order to confirm this analysis we would have to calculate the optical conductivity for all regimes of frequency which would mean going beyond the large-momentum expansion used above for the propagators. We do not have a clear evaluation of this physics, but at least the conclusion seems indeed to be that curvature effects should contribute positively to the minimal DC conductivity of graphene. This is in line with the arguments and expectations of Ref. [43].

Let us now turn our attentions to the $M_e^2 < 0$ case. The optical conductivity reads now

$$\sigma^{jk}(z, x') = \frac{e^2}{2}\left[\frac{4}{\pi}\frac{1}{z + i\tau_-^{-1}(z)} + 1 + \frac{i}{\pi}\ln\left(\frac{z + i\tau_-^{-1} + 2i}{z + i\tau_-^{-1} - 2i}\right)\right]. \tag{3.79}$$

Fig. 3.4a describes the non-interacting optical conductivity ($\tau_-^{-1} = 0$ above). Here the model seems to run into trouble with the Kramers-Kronig relations as pointed out by the vanishing of the imaginary component. In comparison with Eq. (3.75), we note the source of its imaginary component is solely due to the first term, i.e., the intraband transitions. For $M_e^2 < 0$ (and $\tau_-^{-1} = 0$) this term becomes purely real. Inclusion of broadening effects seems to lift the problem as shown in Fig. 3.4b. Here the real component also assumes a form similar to Ref. [115] although it always stays very close to σ_0 after it crosses it from the above.

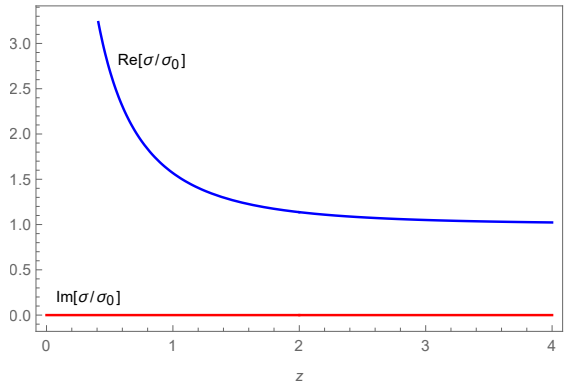

(a) Real and imaginary parts of non-interacting optical conductivity normalized to σ_0.

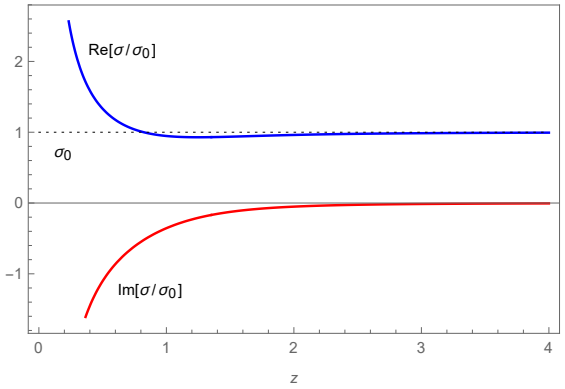

(b) Real and imaginary parts of optical conductivity normalized to σ_0 with broadening effects.

Figure 3.4: Conductivity in graphene with for negative Ricci scalar.

Chapter 4

Conclusions

In the first part of this work we developed a formalism to study the curved-space RQED by employing the local momentum representation. Then we applied the model, with slight modifications, to graphene. In particular the optical conductivity was computed to one-loop and at leading adiabatic order revealing the appearance of an effective chemical potential for the positive Ricci scalar case. Importantly this effect is non-perturbative as it stems from the partial ressumation of the Ricci scalar. Furthermore, we demonstrated how the combined effect of the ripples of the graphene sheet (modeled here by curvature effects) and electron-electron interactions as described by the curved-space RQED could be responsible for the minimal DC conductivity. Even taking into account the limitations of the present model, this conclusion seems to be true.

There are many open questions outside our scope that are nonetheless of great importance. Most obvious is developing curved space RQED beyond the approximations presented here for the local momentum space representation. In particular it would be interesting to investigate whether such higher order corrections can impact the density of states. It is known that around a defect the local density of states is either enhanced or suppressed according to the whether the curvature is positive or negative [35]. Another matter that has been left out of this work was the treatment of dislocations. The local momentum space representation does not take torsion into account, thus a generalization of the method is needed. This issue was tackled in [117], thus it seems like a natural path to take. Within our approach it would also be interesting to study the trace anomaly and conformal invariance of the model. Research into possible holographic models (both for flat and curved RQED) would be most welcome for providing a tool into the non-perturbative regime. Furthermore boundary CFTs within holography have seen some interesting recent activity, see, e.g. [118]. A two-loop analysis is also desirable specially for a more rigorous account of electron-electron interaction contributions to the optical conductivity for a better comparison with the literature [43]. Additionally a computation of the global conductivity $\sigma(\omega)$ from the local $\sigma(\omega, x')$ by a disorder averaging treatment of $M_e^2(x')$ is expected to accurately model real samples. We hope to access these issues in future works.

Appendix A

Riemann normal coordinates expansion

The construction of Riemann normal coordinates about some point x' in the manifold goes as follows. On x' it is possible to make $g_{\mu\nu}(x') = \eta_{\mu\nu}(x')$ along with $\Gamma^{\alpha}_{\ \mu\nu}(x') = 0$. Now suppose that points x in the neighborhood of x' can be reached by a unique geodesic starting from x'. This is the so-called normal neighborhood of x'. We can make use of the tangent vectors to the geodesics to introduce a normal coordinate system X^{μ} with origin at x' such that

$$\frac{d^2 X^{\alpha}}{d\lambda^2} = 0 \tag{A.1}$$

along any geodesic, with λ some affine parameter describing the geodesic. By expanding with respect to these coordinates one finds that [109, 119]

$$\begin{aligned}
g_{\mu\nu}(x) &= \eta_{\mu\nu} - \frac{1}{3} R_{\mu\rho\sigma\nu}(x') X^{\rho} X^{\sigma} + \cdots \\
(-g(x))^{1/2} &= 1 + \frac{1}{6} R_{\mu\nu}(x') X^{\mu} X^{\nu} + \cdots \\
\Gamma_{\mu\ j}^{\ i}(x) &= -\frac{1}{4} R_{\mu\rho ab}(x') (J^{ab})^{i}_{\ j} X^{\rho} + \cdots \\
Q^{i}_{\ j}(x) &= Q^{i}_{\ j}(x') + \cdots \\
e_{a}^{\ \mu}(x) &= e_{a}^{\ \nu}(x') \left(\delta^{\mu}_{\nu} + \frac{1}{6} R_{\nu\alpha\ \beta}^{\ \mu}(x') X^{\alpha} X^{\beta} \right) + \cdots
\end{aligned} \tag{A.2}$$

where only the lowest-order terms are retained. Here $R_{\mu\rho ab}$ is the Riemann curvature tensor with two vielbein indices and J^{ab} is the Lorentz generator for the representation appropriate to the field under consideration. Also $Q^{i}_{\ j}$ is a quantity proportional to the curvature. Let us derive the expansion for the spin connection. From Eq. (A.2), one finds

$$\omega_{\mu ab} = -\frac{1}{2} R_{\mu\rho ab}(x') X^{\rho} \tag{A.3}$$

where we used the cyclicity property of the Riemann tensor. Then

$$\Omega_{\mu} = \frac{1}{2} \omega_{\mu ab} J^{ab} = -\frac{1}{4} R_{\mu\rho ab}(x') X^{\rho} J^{ab} = -\frac{1}{8} R_{\mu\rho ab}(x') \gamma^{a} \gamma^{b} X^{\rho} \tag{A.4}$$

which implies that

$$\gamma^{\mu}(x) \nabla_{\mu} = \gamma^{a} e_{a}^{\ \mu}(x) (\partial_{\mu} + \Omega_{\mu}) = \gamma^{\nu}(x') \left(\partial_{\nu} + \frac{1}{6} R^{\mu}_{\ \alpha\nu\beta}(x') X^{\alpha} X^{\beta} \partial_{\mu} - \frac{1}{8} R_{ab\nu\rho}(x') \gamma^{a} \gamma^{b} X^{\rho} \right). \tag{A.5}$$

However, using the anticommutation relations for the gamma matrices and again the cyclicity property of the Riemann tensor, one finds that

$$R_{abc\rho} \gamma^{c} \gamma^{a} \gamma^{b} = 2 R_{a\rho} \gamma^{a}$$

which yields

$$\gamma^{\mu}(x) \nabla_{\mu} = \gamma^{\nu}(x') \left(\partial_{\nu} + \frac{1}{6} R^{\mu}_{\ \alpha\nu\beta}(x') X^{\alpha} X^{\beta} \partial_{\mu} - \frac{1}{4} R_{\nu\rho}(x') X^{\rho} \right). \tag{A.6}$$

A.1 Local-momentum representation of the fermionic propagator

In this Appendix we consider the local-momentum representation for the fermion propagator. The standard representation has been extensively discussed in the literature, see for instance Refs. [109, 120, 121]. Tipically, since curvature effects are small, we will be interested only in the leading terms in the Riemann curvature. But for the moment we will keep our discussion as general as possible. In principle, we could follow the same steps outlined above. There is, however, another alternative form of proper-time expansion for propagators in curved space-time which could be useful here. It is based on a partial resummation of the above series [122]. Consider Eq. (3.31) with $\vartheta = -1$. One can write the Green's function as

$$G(x,x') = -i\int_0^\infty ds\langle x,s|x',0\rangle \tag{A.7}$$

where we omitted matrix indices, and the kernel $\langle x,s|x',0\rangle$ has a Schwinger-DeWitt expansion given by [123]

$$\begin{aligned}\langle x,s|x',0\rangle &= i(4\pi is)^{-d/2}e^{i\sigma(x,x')/2s}\Delta^{1/2}_{\rm VM}(x,x')F(x,x';is)\\ F(x,x';is) &= \mathbf{1}+\sum_{j=1}^\infty (is)^j f_j(x,x')\end{aligned} \tag{A.8}$$

where $2\sigma(x,x')$ is the square of the proper arc length along the geodesic from x' to x and $\Delta_{\rm VM}(x,x')$ is the Van Vleck-Morette determinant defined by [124]

$$\Delta_{\rm VM}(x,x') = -|g(x)|^{-1/2}|g(x')|^{-1/2}\det\left[-\frac{\partial^2\sigma(x,x')}{\partial x^\mu \partial'^\nu}\right]. \tag{A.9}$$

In turn, such an expansion can be rewritten in the form

$$\begin{aligned}\langle x,s|x',0\rangle &= i(4\pi is)^{-d/2}e^{i\sigma(x,x')/2s}\Delta^{1/2}_{\rm VM}(x,x')\bar{F}(x,x';is)e^{-is\left[Q(x')-\frac{1}{6}R(x')\right]}\\ \bar{F}(x,x';is) &= \mathbf{1}+\sum_{j=1}^\infty (is)^j \bar{f}_j(x,x')\end{aligned} \tag{A.10}$$

an assertion which was proved in Ref. [122]. The coefficients $\bar{f}_j(x,x')$ are R independent to all orders, but generically depend on the Ricci curvature and the Riemann tensor and their powers and derivatives. In addition, we stress that such coefficients in the fermionic case should be envisaged as bispinors; hence to perform properly the above expansion one should form the contraction between such bispinors with the bispinor of parallel displacement $\boldsymbol{\sigma}(x,x')$. It can be proved that $\boldsymbol{\sigma}(x,x') = \bar{f}_0(x,x') = \mathbf{1}$ [128].

The term $e^{-is\left[Q(x')-\frac{1}{6}R(x')\mathbf{1}\right]}$ should be defined as a a formal matrix power series ($\mathbf{1}$ is the unit spinor, in the case of fermions). A straightforward calculation yields

$$\begin{aligned}\bar{F}(x,x';is)e^{-is\left[Q(x')-\frac{1}{6}R(x')\mathbf{1}\right]} &= \mathbf{1}+(is)\left(\bar{f}_1(x,x')-A(x')\right)\\ &+ (is)^2\left(\bar{f}_2(x,x')+\frac{1}{2}A^2(x')-\bar{f}_1(x,x')A(x')\right)+\cdots\end{aligned} \tag{A.11}$$

where $A(x') = Q(x') - R(x')/6$. Since such expansions should be equal, one finds that

$$\begin{aligned}\bar{f}_1(x,x') &= f_1(x,x')+A(x')\\ \bar{f}_2(x,x') &= f_2(x,x')-\frac{1}{2}A^2(x')+(f_1(x,x')+A(x'))A(x')\end{aligned} \tag{A.12}$$

and so on. On the other hand, with Riemann normal coordinates y^μ for the point x with origin at the point x', one has that

$$f_1(x,x') = f_1(x')+f_{1\alpha}(x')y^\alpha + f_{1\alpha\beta}(x')y^\alpha y^\beta + \mathcal{O}(y^3)$$

where an expansion about the point x' was considered. The coefficients $f_{j\alpha\beta\ldots}$ are all proportional to derivatives of the f_j evaluated at the origin of the Riemann normal coordinates (i.e., at x'). The coefficients f_j have been calculated in the literature [128]. In particular, $\bar{f}_1 = 0$.

Now use the fact that, in Riemann normal coordinates about x', $\Delta_{\rm VM}(x,x') = |g(x)|^{-1/2}$, together with the results

$$\int \frac{d^Dk}{(2\pi)^D} e^{-is(-k^2+m^2)-iky} = i(4\pi is)^{-d/2} e^{i\sigma(x,x')/2s} e^{-ism^2} \tag{A.13}$$

where $\sigma(x,x') = -y_\alpha y^\alpha/2$, and

$$\int_0^\infty ids\, e^{-is(-k^2+m^2)} = \frac{1}{-k^2+m^2}$$

to obtain that

$$G(x,x') = \Delta^{1/2}_{\rm VM}(x,x') \int \frac{d^Dk}{(2\pi)^D} e^{-iky} \bar{F}\left(x,x';-\frac{\partial}{\partial m^2}\right) \frac{1}{k^2-m^2} \tag{A.14}$$

where $m^2 = Q(x') - R(x')/6$ (Q now is just a function). Here $D = d_e$ for the case of the fermionic propagator. We also consider the replacement

$$y^\alpha \to i\frac{\partial}{\partial k_\alpha} \tag{A.15}$$

in the above expression.

Now we are in the position of presenting an explicit expression for the fermionic propagator using Riemann normal coordinates about x'. Using that $m^2 = M_e^2 = R(x')/12$ for fermions as well as the above expansions for $\Delta_{\rm VM}(x,x')$ and $\gamma^\mu\nabla_\mu$, one finds, for the fermionic propagator

$$\begin{aligned} S_0(x,x') &= \int \frac{d^Dk}{(2\pi)^D} e^{-iky}\left[\frac{\gamma^\nu k_\nu}{k^2-M_e^2} + \frac{1}{(k^2-M_e^2)^2}\left(\frac{1}{2}R_{\nu\rho}\gamma^\nu k^\rho - \frac{\gamma^\nu k_\nu}{6}R\right)\right. \\ &+ \left.\frac{2}{3}\frac{\gamma^\nu k_\nu k^\sigma k^\rho R_{\rho\sigma}}{(k^2-M_e^2)^3} + \cdots\right] \end{aligned} \tag{A.16}$$

where in the above equation γ^μ is the usual gamma matrix in flat space and $R = R_{\mu\nu}\eta^{\mu\nu}$ when considering only terms linear in the curvature for the expansion of $g^{\mu\nu}$ in Riemann normal coordinates.

A.2 Local-momentum representation of the gauge propagator

In this Appendix we present the local-momentum representation of the gauge propagator. For a standard discussion, see for instance Refs. [109,119,125]. In the present case, one has that the gauge propagator obeys

$$[\eta_{\mu\lambda}\Box + R_{\mu\lambda}]G^\lambda_{\nu'} = \eta_{\mu\nu'}\delta(x,x'). \tag{A.17}$$

Following [122,126] one has, for the gauge propagator (in the Feynman gauge $\xi = 1$)

$$G^\mu{}_{\nu'}(x,x') = i\int_0^\infty ds\langle x,s|x',0\rangle^\mu{}_{\nu'} \tag{A.18}$$

with

$$\begin{aligned} \langle x,s|x',0\rangle^\mu{}_{\nu'} &= i(4\pi is)^{-d/2} e^{i\sigma(x,x')/2s}\Delta^{1/2}_{\rm VM}(x,x')\bar{H}^\mu{}_{\nu'}(x,x';is)e^{isR(x')/6} \\ \bar{H}^\mu{}_{\nu'}(x,x';is) &= g^\mu{}_{\nu'}(x,x') + \sum_{j=1}^\infty (is)^j \bar{h}_j{}^\mu{}_{\nu'}(x,x') \end{aligned} \tag{A.19}$$

We stress that $\bar{h}_j{}^\mu{}_{\nu'}$ is a bivector. Recall that, for a proper expansion of a bivector, such as the gauge propagator, one must form the combination $g^\nu{}_{\lambda'}G^{\mu\lambda'}$, which is a contravariant tensor of rank two at x and a scalar at x'. The object $g^\nu{}_{\lambda'}$ is the bivector of parallel transport from x' to x [127]. Note that $g_{\mu\nu'}(x,x) = g_{\mu\nu}$.

Proceeding with analogous considerations as above, one obtains that

$$\begin{aligned} \bar{h}_1{}^\mu{}_{\nu'}(x') &= h_1{}^\mu{}_{\nu'}(x') + B(x')g^\mu{}_{\nu'} \\ \bar{h}_{1\alpha}{}^\mu{}_{\nu'}(x') &= h_{1\alpha}{}^\mu{}_{\nu'}(x') \\ \bar{h}_{1\alpha\beta}{}^\mu{}_{\nu'}(x') &= h_{1\alpha\beta}{}^\mu{}_{\nu'}(x') \\ \bar{h}_2{}^\mu{}_{\nu'}(x') &= h_2{}^\mu{}_{\nu'}(x') + \frac{1}{2}B^2(x')g^\mu{}_{\nu'} + B(x')h_1{}^\mu{}_{\nu'}(x') \end{aligned} \tag{A.20}$$

where $B(x') = -R(x')/6$, $\bar{h}_1{}^{\mu}{}_{\nu'}(x,x') = \bar{h}_1{}^{\mu}{}_{\nu'}(x') + \bar{h}_{1\alpha}{}^{\mu}{}_{\nu'}(x')y^{\alpha} + \bar{h}_{1\alpha\beta}{}^{\mu}{}_{\nu'}(x')y^{\alpha}y^{\beta} + \mathcal{O}(y^3)$. Here the coefficients $h_j{}^{\mu}{}_{\nu'}$ can also be found in the literature [127].

As above, we are interested only in terms linear in the Riemann curvature. Using Riemann normal coordinates about x', one obtains

$$G_{\mu\nu'}(x,x') = -\Delta^{1/2}_{\rm VM}(x,x')\int \frac{d^{d_\gamma}k}{(2\pi)^{d_\gamma}} e^{-iky}\bar{H}_{\mu\nu'}\left(x,x';-\frac{\partial}{\partial M^2_\gamma}\right)\frac{1}{k^2-M^2_\gamma} \tag{A.21}$$

where $M^2_\gamma = -R(x')/6$ and we used that [126]

$$g_{\mu\nu'}(x,x') = \eta_{\mu\nu'} - \frac{1}{6}R_{\mu\rho\sigma\nu'}(x')y^{\rho}y^{\sigma} + \cdots . \tag{A.22}$$

By using the aforementioned expansion for the Van Vleck-Morette determinant, together with previous results, one finds that

$$\begin{aligned} G_{\mu\nu'}(x,x') &= -\int \frac{d^{d_\gamma}k}{(2\pi)^{d_\gamma}} e^{-iky}\left[\frac{\eta_{\mu\nu'}}{k^2-M^2_\gamma} + \frac{1}{(k^2-M^2_\gamma)^2}\left(\frac{2}{3}R_{\mu\nu'} - \frac{1}{6}R\eta_{\mu\nu'}\right)\right. \\ &- \left.\frac{2}{3}\frac{(2R_{\mu\alpha\beta\nu'} - R_{\alpha\beta}\eta_{\mu\nu'})k^{\alpha}k^{\beta}}{(k^2-M^2_\gamma)^3} + \cdots\right]. \end{aligned} \tag{A.23}$$

Recall that the gauge propagator obtained above corresponds to the one in d_γ dimensions. Since here we are interested in the properties of the system in the reduced space where the fermion field is living, we integrate over the $d_\gamma - d_e$ bulk gauge degrees of freedom.

Bibliography

[1] S. Nadj-Perge *et al.*, "Observation of Majorana fermions in ferromagnetic atomic chains on a superconductor", Science **346**, 602 (2014), [arXiv:1410.0682 [cond-mat.mes-hall]].

[2] S.-Y. Xu *et al.*, "Discovery of a Weyl fermion semimetal and topological Fermi arcs", Science **349**, 613 (2015) [arXiv:1502.03807 [cond-mat.mes-hall]].

[3] W. G. Unruh, "Experimental black hole evaporation", Phys. Rev. Lett. **46**, 1351 (1981)

[4] U. Leonhardt and P. Piwnicki , "Relativistic Effects of Light in Moving Media with Extremely Low Group Velocity", Phys. Rev. Lett. **84**, 822 (2000) [arXiv:cond-mat/9906332 [cond-mat.soft]].

[5] L. J. Garay, J. R. Anglin, J. I. Cirac and P. Zoller, "Sonic Analog of Gravitational Black Holes in Bose-Einstein Condensates", Phys. Rev. Lett. **85**, 4643 (2000) [arXiv:gr-qc/0002015].

[6] B. Horstmann, B. Reznik, S. Fagnocchi S. and J. I. Cirac, "Hawking Radiation from an Acoustic Black Hole on an Ion Ring", Phys. Rev. Lett. **104**, 250403 (2010) [arXiv:0904.4801 [quant-ph]].

[7] A. Recati, N. Pavlov and I. Carusotto, "Bogoliubov theory of acoustic Hawking radiation in Bose-Einstein condensates", Phys. Rev. A **80**, 043603 (2009) [arXiv:0907.4305 [cond-mat.quant-gas]].

[8] C. Mayoral, A. Fabbri and M. Rinaldi, "Steplike discontinuities in Bose-Einstein condensates and Hawking radiation: Dispersion effects", Phys. Rev. D **83**, 124047 (2011) [arXiv:1008.2125 [gr-qc]].

[9] G. Menezes and J. Marino, "Slow scrambling in sonic black holes", EPL **121**, 60002 (2018) [arXiv:1712.05456 [cond-mat.quant-gas]].

[10] S. Basak and P. Majumdar, "'Superresonance' from a rotating acoustic black hole", Class. Quantum Grav. **20**, 3907 (2003) [arXiv:gr-qc/0203059].

[11] T. R. Slatyer and C. M. Savage, "Superradiant scattering from a hydrodynamic vortex", Class. Quantum Grav. **22**, 3833 (2005) [arXiv:cond-mat/0501182 [cond-mat.other]].

[12] V. Cardoso, A. Coutant, M. Richartz and S. Weinfurtner, "Detecting Rotational Superradiance in Fluid Laboratories", Phys. Rev. Lett. **117**, 271101 (2016) [arXiv:1607.01378 [gr-qc]].

[13] L. Giacomelli and S. Liberati, "Rotating black hole solutions in relativistic analogue gravity", Phys. Rev. D 96, 064014 (2017) [arXiv:1705.05696 [gr-qc]].

[14] D. Faccio and E. M. Wright, "Superradiant Amplification of Acoustic Beams via Medium Rotation", Phys. Rev. Lett. **123**, 044301 (2019) [arXiv:1809.03489 [physics.class-ph]].

[15] M. C. Braidotti, A. Vinante, G. Gasbarri, D. Faccio and H. Ulbricht, "Zel'dovich Amplification in a Superconducting Circuit", Phys. Rev. Lett. **125**, 140801 (2020) [arXiv:2005.03705 [physics.class-ph]].

[16] L. Giacomelli and I. Carusotto, "Ergoregion instabilities in rotating two-dimensional Bose-Einstein condensates: Perspectives on the stability of quantized vortices", Phys. Rev. Research **2**, 033139 (2020) [arXiv:2006.09259 [cond-mat.quant-gas]].

[17] J. Marino, G. Menezes, and I. Carusotto, "Zero-point excitation of a circularly moving detector in an atomic condensate and phonon laser dynamical instabilities", Phys. Rev. Research **2**, 042009(R) (2020) [arXiv:2001.08646 [cond-mat.quant-gas]].

[18] K. Novoselov *et al.*, "Two-dimensional gas of massless Dirac fermions in graphene", Nature **438**, 197 (2005) [arXiv:cond-mat/0509330 [cond-mat.mes-hall]].

[19] Y. Zhang, Y.-W. Tan, H. L. Stormer and P. Kim, "Experimental Observation of Quantum Hall Effect and Berry's Phase in Graphene", Nature **438**, 201 (2005) [arXiv:cond-mat/0509355 [cond-mat.mes-hall]].

[20] N. Stander, B. Huard, and D. Goldhaber-Gordon "Evidence for Klein Tunneling in Graphene p-n Junctions", Phys. Rev. Lett. **102**, 026807 (2009).

[21] A. Young and P. Kim, "Quantum interference and Klein tunnelling in graphene heterojunctions", Nature Phys. **5**, 222 (2009).

[22] K. Novoselov *et al.*, "Room-Temperature Quantum Hall Effect in Graphene", Science **315**, 1379 (2007) [arXiv:cond-mat/0702408 [cond-mat.mes-hall]].

[23] M. Katsnelson, K. Novoselov and A. Geim, "Chiral tunnelling and the Klein paradox in graphene", Nature Phys. **2**, 620 (2006).

[24] K. S. Novoselov *et al.*, "Electric Field Effect in Atomically Thin Carbon Films", Science **306**, 666 (2004) [arXiv:cond-mat/0410550 [cond-mat.mtrl-sci]].

[25] X. Du, I. Skachko, F. Duerr, A. Luican, and E. Y. Andrei, "Fractional quantum Hall effect and insulating phase of Dirac electrons in graphene", Nature **462**, 192 (2009) [arXiv:0910.2532 [cond-mat.mes-hall]].

[26] K. l. Bolotin, F. Ghahari, M. D. Shulman, H. L. Stormer, and P. Kim, "Observation of the fractional quantum Hall effect in graphene", Nature **462**, 196 (2009) [arXiv:0910.2763 [cond-mat.mes-hall]].

[27] F. Ghahari, Y. Zhao, P. Cadden-Zimansky, K. Bolotin, P. Kim, "Measurement of the $\nu = 1/3$ Fractional Quantum Hall Energy Gap in Suspended Graphene", Phys. Rev. Lett. **106**, 046801 (2011) [arXiv:1010.1187 [cond-mat.mes-hall]].

[28] C. R. Dean *et al.*, "Multicomponent fractional quantum Hall effect in graphene", Nat. Phys. **7**, 693 (2011) [arXiv:1010.1179 [cond-mat.mes-hall]].

[29] M. S. Foster and I. L. Aleiner, "Graphene via large N: A renormalization group study", Phys. Rev. B **77**, 195413 (2008) [arXiv:0802.0283 [cond-mat.dis-nn]].

[30] Y. Seo, G. Song, P. Kim, S. Sachdev, and S.-J. Sin, "Holography of the Dirac Fluid in Graphene with Two Currents", Phys. Rev. Lett. **118**, 036601 (2017) [arXiv:1609.03582v2 [hep-th]].

[31] A. Iorio and G. Lambiase, "The Hawking-Unruh phenomenon on graphene", Phys. Lett. B **716**, 334 (2012) [arXiv:1108.2340 [cond-mat.mtrl-sci]].

[32] A. Iorio and G. Lambiase, "Quantum field theory in curved graphene spacetimes, Lobachevsky geometry, Weyl symmetry, Hawking effect, and all that", Phys. Rev. D **90**, 025006 (2014) [arXiv:1308.0265 [hep-th]].

[33] M. Cvetic and G.W Gibbons, "Graphene and the Zermelo optical metric of the BTZ black hole", Ann. Phys. **327**, 2617 (2012). [arXiv:1202.2938 [hep-th]].

[34] F. de Juan, A. Cortijo and M. A. H. Vozmediano, "Charge inhomogeneities due to smooth ripples in graphene sheets", Phys. Rev. B **76**, 165409 (2007) [arXiv:0706.0176 [cond-mat.str-el]].

[35] A. Cortijo and M. A.H. Vozmediano, "Effects of topological defects and local curvature on the electronic properties of planar graphene", Nucl. Phys. B **763** [FS], 293 (2007) [arXiv:cond-mat/0612374 [cond-mat.str-el]].

[36] A. Iorio and P. Pais, "Revisiting the gauge fields of strained graphene", Phys. Rev. D **92**, 125005 (2015) [arXiv:1508.00926 [hep-th]].

[37] E. Arias, A. R. Hernández and C. Lewenkopf, "Gauge fields in graphene with nonuniform elastic deformations: A quantum field theory approach", Phys. Rev. B **92**, 245110 (2015) [arXiv:1511.08639 [cond-mat.mes-hall]].

[38] M. A. H. Vozmediano, M. I. Katsnelson and F. Guinea, "Gauge fields in graphene", Phys. Rep. **496**, 109 (2010) [arXiv:1003.5179 [cond-mat.mes-hall]].

[39] X. Du, I. Skachko, A. Barker, and E. Y. Andrei, "Approaching Ballistic Transport in Suspended Graphene", Nat. Nanotechnol. 3, 491 (2008) [arXiv:0802.2933 [cond-mat.mes-hall]].

[40] S. Teber, *Field theoretic study of electron-electron interaction effects in Dirac liquids*. PhD Thesis [arXiv:1810.08428 [cond-mat.mes-hall]].

[41] E. C. Marino, "Quantum electrodynamics of particles on a plane and the Chern-Simons theory", Nucl. Phys. B **408**, 551 (1993) [arXiv:hep-th/9301034].

[42] E. V. Gorbar, V. P. Gusynin, and V. P. Miransky, "Dynamical Chiral Symmetry Breaking on a Brane in Reduced QED", Phys. Rev. D 64, 105028 (2001) [arXiv:1609.05577].

[43] E. C. Marino, L. O. Nascimento, V. S. Alves and C. M. Smith, "Interaction Induced Quantum Valley Hall Effect in Graphene", Phys. Rev. X **5**, 011040 (2015) [arXiv:1309.5879 [cond-mat.str-el]].

[44] S. Teber, "Electromagnetic current correlations in reduced quantum electrodynamics", Phys. Rev. D **86**, 025005 (2012) [arXiv:1204.5664 [hep-ph]].

[45] D. Dudal, A. J. Mizher and P. Pais, "Comments on the Chern-Simons photon term in the QED description of graphene", Phys. Rev. D **98**, 065008 (2018) [arXiv:1801.08853 [hep-th]].

[46] D. Dudal, A. J. Mizher and P. Pais, "On the exact quantum scale invariance of three-dimensional reduced QED theories", Phys. Rev. D **99**, 045017 (2019) [arXiv:1808.04709 [hep-th]].

[47] J. B. Cuevas, A. Raya and J. C. Rojas, "Chiral symmetry restoration in reduced QED at finite temperature in the supercritical coupling regime", Phys. Rev. D **102**, 056020 (2020) [arXiv:2007.05652 [hep-th]].

[48] J. A. C. Olivares, L. Albino, A. J. Mizher and A. Raya, "Influence of a Chern-Simons term in the dynamical fermion masses in reduced or pseudo QED", Phys. Rev. D **102**, 096023 (2020) [arXiv:2009.08484 [hep-ph]].

[49] P. I. C. Caneda and G. Menezes, "Reduced quantum electrodynamics in curved space", Phys. Rev. D **103**, 065010 (2021) [arXiv:2011.09500 [cond-mat.mes-hall]]

[50] N. D. Birrell and P. C. W. Davies, *Quantum Fields in Curved Space* (Cambridge University Press, Cambridge, England, 1982).

[51] L. Parker and D. Toms, *Quantum Field Theory in Curved Spacetime* (Cambridge University Press, Cambridge, England, 2009).

[52] A. Z. Petrov, *Einstein Spaces* (Pergamon, Oxford, 1969).

[53] L. Parker, in *Proceedings of the NATO Advanced Study Institute on Gravitation: Recent Developments*, edited by M. Levy and S. Deser (Plenum, New York, 1979).

[54] P. R. Wallace, "The band theory of graphite", Phys. Rev. **71**, 622 (1947)

[55] J. W. McClure, "Band structure of graphite and de Haas-van Alphen effect", Phys. Rev. **108**, 612 (1957)

[56] J. C. Slonczewski and P. R. Weiss, "Band structure of graphite", Phys. Rev. **109**, 272 (1958)

[57] W. S. Boyle and P. Nozières, "Band structure and infrared absorption of graphite", Phys. Rev. **111**, 782 (1958)

[58] J. W. McClure, "Analysis of multicarrier galvanomagnetic data for graphite", Phys. Rev. **112**, 715 (1958)

[59] W. J. Spry and P. M. Scherer, "de Haas-van Alphen effect in graphite between 3 and 85 kilogauss", Phys. Rev. **120**, 826 (1960)

[60] D. E. Soule, J. W. McClure and L. B. Smith, "Study of Shubnikov-de Haas effect. Determination of the Fermi surfaces in graphite", Phys. Rev. **134**, A453 (1964)

[61] S. J. Williamson, S. Forner and M. S. Dresselhaus, "de Haas-van Alphen effect in pyrolytic and single-crystal graphite", Phys. Rev. **140**, A1429 (1965)

[62] D. P. DiVincenzo and E. J. Mele, "Self-consistent effective-mass theory for intralayer screening in graphite intercalation compounds", Phys. Rev. B **29**, 1685 (1984)

[63] G. W. Semenoff "Condensed-Matter Simulation of a Three-Dimensional Anomaly", Phys. Rev. Lett. **53**, 2449 (1984)

[64] E. Schrödinger, Preuss. Akad. Wiss. Phys. Math. Kl. **24**, 418 (1930)

[65] A. O. Barut and A. J. Bracken, "Zitterbewegung and the internal geometry of the electron ", Phys. Rev. D **23**, 2454 (1981)

[66] R. Gerritsma, G. Kirchmair, F. Zähringer, E. Solano, R. Blatt and C. F. Roos, "Quantum simulation of the Dirac equation", Nature **463**, 68 (2010)

[67] T. M. Rusin and W. Zawadzki, "Zitterbewegung of electrons in graphene in a magnetic field ", Phys. Rev. B **78**, 125419 (2008) [arXiv:0712.3590 [cond-mat.mes-hall]]

[68] A. Castro Neto, F. Guinea, N. Peres, K. Novoselov and A. Geim, "The electronic properties of graphene", Rev. Mod. Phys. **81**, 109 (2009).

[69] M. Katsnelson "The physics of graphene", CUP, 2020.

[70] Andrei Bernervig and Taylor L. Hughes, "Topological Insulators and topological superconductors", PUP, 2013

[71] J. L. Mañes, F. Guinea and María A. H. Vozmediano, "Existence and topological stability of Fermi points in multilayered graphene", Phys. Rev. B **75**, 155424 (2007) [arXiv:cond-mat/0611347].

[72] A. Hashimoto *et al.*, "Direct evidence for atomic defects in graphene layers", Nature **430**, 870 (2004).

[73] S. V. Morozov, K. S. Novoselov, M. I. Katsnelson, F. Schedin, L. A. Ponomarenko, D. Jiang, and A. K. Geim, "Strong Suppression of Weak Localization in Graphene", Phys. Rev. Lett. **97**, 016801 (2006).

[74] J. C. Meyer, A. K. Geim, M. I. Katsnelson, K. S. Novoselov, T. J. Booth and S. Roth, "The structure of suspended graphene sheets", Nature **446**, 60 (2007) [arXiv:cond-mat/0701379 [[cond-mat.mes-hall]]].

[75] J. C. Meyer, A. K. Geim, M. I. Katsnelson, K. S. Novoselov, D. Obergfell, S. Roth, C. Girit and A. Zettl, "On the roughness of single- and bi-layer graphene membranes", Solid State Communications **143**, 101 (2007) [arXiv:cond-mat/0703033 [cond-mat.mes-hall]].

[76] M. Ishigami, J. H. Chen, W. G. Cullen, M. S. Fuhrer, and E. D. Williams, "Atomic Structure of Graphene on SiO2", Nano Letters **7**, 1643 (2007) [arXiv:0811.0587 [cond-mat.mtrl-sci]].

[77] E. Stolyarova, K. T. Rim, S. Ryu, J. Maultzsch, P. Kim, L. E. Brus, T. F. Heinz, M. S. Hybertsen, and G. W. Flynn, "High-resolution scanning tunneling microscopy imaging of mesoscopic graphene sheets on an insulating surface", PNAS **104**, 9209 (2007) [arXiv:0705.0833 [cond-mat.mes-hall]].

[78] K. Suenaga, H. Wakabashi, M. Koshino, Y. Sato, K. Urita and S. Iijima, "Imaging active topological defects in carbon nanotubes", Nature Nanotechnology **2**, 358 (2007).

[79] A. Fasolino, J. H. Los, M. I. Katsnelson, "Intrinsic ripples in graphene", Nature Materials **6**, 858 (2007) [arXiv:0704.1793 [cond-mat.mtrl-sci]].

[80] J. C. Meyer *et al.*, "Direct Imaging of Lattice Atoms and Topological Defects in Graphene Membranes", Nano Lett. **8**, 3582 (2008).

[81] J. Pachos and M. Stone, "An index theorem for graphene", Int. J. Mod. Phys. B **21**, 5113 (2007)

[82] M. O. Katanaev, I. V. Volovich, "Theory of elastic defects in solids and three-dimensional gravity", Ann. of Phys. **216**, 1 (1992).

[83] D. M. McAvity and H. Osborn "Conformal field theories near a boundary in general dimensions", Nucl. Phys. B **455**, 522 (1993) [arXiv:cond-mat/9505127]

[84] C. P. Herzog and K. W. Huang, "Boundary conformal field theory and a boundary central charge", JHEP **10**, 189 (2017) [arxiv:1707.06224[hep-th]]

[85] A. Karch and Y. Sato, "Conformal manifolds with boundaries or defects", JHEP **7**, 156 (2018) [arxiv:1805.10427[hep-th]]

[86] N. Menezes, G. Palumbo and C. M. Smith, "Conformal QED in two-dimensional topological insulators", Scientific Reports **7**, 14175 (2017) [arXiv:mes-hall/]

[87] D. G. Barci, C. G. Bollini, L. E. Oxman, M. C. Rocca, "Non-local pseudo-differential operators" [arXiv:hep-th/9606183]

[88] D. G. Barci, L. E. Oxman and M. Rocca, "Canonical quantization of nonlocal field equations", Int. J. Mod. Phys. A **11**, 2111 (1996) [arXiv:hep-th/9503101]

[89] D. G. Barci, L. E. Oxman, "Asymptotic States in Nonlocal Field Theories", Int. J. Mod. Phys. **12**, 493 (1997) [arXiv:hep-th/9611147]

[90] E. C. Marino, L. O. Nascimento, V. S. Alves and C. M. Smith, "Unitarity of theories containing fractional powers of the d'Alembertian operator", Phys. Rev. D **90**, 105003 (2014) [arXiv:1408.1637]

[91] Y. Pará, V. S. Alves, T. Macrì, E. C. Marino and L. O. Nascimento "Bosonic interactions in a nonlocal theory in (2+1) dimensions", Phys. Rev. D **100**, 085010 (2019) [arXiv:1906.08334]

[92] V. S. Alves, W. S. Elias, L. O. Nascimento, V. Juričić and F. Peña, "Chiral symmetry breaking in the pseudo-quantum electrodynamics", Phys. Rev. D **87**, 125002 (2013)

[93] L. O. Nascimento, V. S. Alves, F. Peña, C. M. Smith, and E. C. Marino, "Chiral-symmetry breaking in pseudoquantum electrodynamics at finite temperature", Phys. Rev. D **92**, 025018 (2015) [arXiv:1503.08347]

[94] V. S. Alves, T. Macri, G. C. Magalhães, E. C. Marino, and L. O. Nascimento "Two-dimensional Yukawa interactions from nonlocal Proca quantum electrodynamics", Phys. Rev. D **97**, 096003 (2018) [arXiv:1712.06401]

[95] V. S. Alves, R. O. C. Junior, E. C. Marino, and L. O. Nascimento "Dynamical mass generation in pseudoquantum electrodynamics with four-fermion interactions", Phys. Rev. D **96**, 034005 (2017) [arXiv:1704.00381]

[96] W. P. Pires, J. D. L. Silva, A. N. Braga, V. S. Alves, D. T. Alves and E. C. Marino "Cavity effects on the Fermi velocity renormalization in a graphene sheet", Nucl. Phys. B **932**, 529 (2018)

[97] G. C. Magalhães, V. S. Alves, E. C. Marino and L. O. Nascimento "Pseudo quantum electrodynamics and Chern-Simons theory coupled to two-dimensional electrons", Phys. Rev. D **101**, 116005 (2020) [arXiv:2001.05378]

[98] G. C. Magalhães, V. S. Alves, L. O. Nascimento and E. C. Marino "Bosonization, mass generation, and the pseudo-Chern-Simons action", Phys. Rev. D **103**, 116022 (2021) [arXiv:2104.01416]

[99] D. Dudal, A. J. Mizher and P. Pais, "The exact quantum scale invariance of three-dimensional reduced QED theories", Phys. Rev. D **99**, 045017 (2019)

[100] J.González, F. Guinea, M.A.H.Vozmediano, "Non-Fermi liquid behavior of electrons in the half-filled honeycomb lattice (A renormalization group approach)" Nucl. Phys. B **424**, 595 (1994) [arXiv:9311105 [hep-th]]

[101] M.A.H.Vozmediano, "Renormalization group aspects of graphene" Phil. Trans. R. Soc. A **369**, 2625 (2011) [arXiv:1010.5057 [cond-mat.str-el]].

[102] J. González, F. Guinea, M.A.H.Vozmediano, "Marginal Fermi Liquid behavior from 2d Coulomb interaction", Phys. Rev. B **59**, 2474 (1999) [arXiv:1010.5057 [cond-mat.str-el]].

[103] J. Hofmann, E. Barnes and S. Das Sarma "Why Does Graphene Behave as a Weakly Interacting System?", Phys. Rev. Lett **113**, 105502 (2014) [arXiv:1405.7036].

[104] Eduardo Fradkin, "Field theories of condensed matter physics", CUP, 2013.

[105] A. Altland and B. Simons, "Condensed Matter Field Theory", CUP, 2006.

[106] W. Kohn, "Cyclotron Resonance and de Haas-van Alphen Oscillations of an Interacting Electron Gas", Phys. Rev. D **123**, 1242 (1961)

[107] R. E. Throckmorton and S. Das Sarma, "Failure of Kohn's theorem and the apparent failure of the f -sum rule in intrinsic Dirac-Weyl materials in the presence of a filled Fermi sea", Phys. Rev. D **98**, 155112 (2018) [arXiv:1805.03650]

[108] S. Coleman and B. Hill, "No More Corrections to the Topological Mass Term in QED3", Phys. Lett. B **159**, 184 (1985)

[109] L. Parker and D. J. Toms, "Renormalization-group analysis of grand unified theories in curved space-time", Phys. Rev. D **29**, 1584 (1984).

[110] P. Panangaden, "One-loop renormalization of quantum electrodynamics in curved spacetime", Phys. Rev. D **23**, 1735 (1981).

[111] J. C. Collins, "Structure of Counterterms in Dimensional Regularization", Nucl. Phys. B **80**, 341 (1974).

[112] T. S. Bunch, "Local Momentum Space and Two-Loop Renormalizability of $\lambda\phi^4$ Field Theory in Curved Space-Time", Gen. Relativ. Gravit. **13**, 711 (1981).

[113] J. F. Donoghue and B. K. El-Menoufi, "Nonlocal quantum effects in cosmology: Quantum memory, nonlocal FLRW equations, and singularity avoidance," Phys. Rev. D **89**, 104062 (2014) [arXiv:1402.3252 [gr-qc]].

[114] G. L. Klimchitskaya, V. M. Mostepanenko, V. M. Petrov, "Conductivity of graphene in the framework of Dirac model: Interplay between nonzero mass gap and chemical potential" Phys. Rev. B **96**, 235432 (2017) [arXiv:1712.04977 [cond-mat.mes-hall]].

[115] T. Ando, Y. Zheng and H. Suzuura, "Dynamical Conductivity and Zero-Mode Anomaly in Honeycomb Lattices" J. Phys. Soc. Jpn. **71**, 1318 (2002).

[116] S. Das Sarma, E. H. Hwang, and W.-K. Tse, "Many-body interaction effects in doped and undoped graphene: Fermi liquid versus non-Fermi liquid," Phys. Rev. B **75**, 121406(R) (2007) [arXiv:cond-mat/0610581 [cond-mat.mes-hall]].

[117] Yu-Huei Wu and Chih-Hung Wang, "Momentum-space representation of the Feynman propagator in Riemann-Cartan spacetime", Phys. Rev. D **82**, 064007 (2010) [arXiv:1004.1777 [gr-qc]].

[118] Rong-Xin Miao, Chong-Sun Chu, and Wu-Zhong Guo, "New proposal for a holographic boundary conformal field theory", Phys. Rev. D **96**, 046005 (2017) [arXiv:1701.04275 [hep-th]]

[119] D. J. Toms, "Local momentum space and the vector field", Phys. Rev. D **90**, 044072 (2014) [arXiv:1408.0636 [hep-th]].

[120] T. Inagaki, T. Muta and S. D. Odintsov, "Nambu-Jona-Lasinio model in curved space-time", Mod. Phys. Lett. A **8**, 2117 (1993) [arXiv:9306023 [hep-th]].

[121] D. J. Toms, "Effective action for the Yukawa model in curved space-time", JHEP **05**, 139 (2018) [arXiv:1804.08350 [hep-th]].

[122] I. Jack and L. Parker, "Proof of summed form of proper-time expansion for propagator in curved space-time", Phys. Rev. D **31**, 2439 (1985).

[123] B. S. DeWitt, in *Relativity, Groups and Topology*, edited by C. DeWitt and B. S. DeWitt (Gordon and Breach, New York, 1964); *Dynamical Theory of Groups and Fields* (Gordon and Breach, New York, 1965).

[124] J. H. Van Vleck, "The Correspondence Principle in the Statistical Interpretation of Quantum Mechanics", Proc. Natl. Acad. Sci. USA **14**, 178 (1928).

[125] I. L. Buchbinder and S. D. Odintsov, "One-Loop renormalization of the Yang-mills field theory in a curved space-time", Sov. Phys. J. **26** (1983) 359.

[126] E. Calzetta, I. Jack and L. Parker, "Quantum gauge fields at high curvature", Phys. Rev. D **33**, 953 (1986).

[127] S. M. Christensen, "Regularization, renormalization, and covariant geodesic point separation", Phys. Rev. D **17**, 946 (1978)

[128] T. S. Bunch and L. Parker, "Feynman propagator in curved spacetime: A momentum-space representation", Phys. Rev. D **20**, 2499 (1979).

[129] L. Parker and D. J. Toms, "Explicit curvature dependence of coupling constants", Phys. Rev. D **31**, 2424 (1985)